UNIVERSITY OF NAPLES FEDERICO II

PH.D. PROGRAM IN

CLINICAL AND EXPERIMENTAL MEDICINE

CURRICULUM IN ODONTOSTOMATOLOGICAL SCIENCES

XXXIII Cycle

(Years 2018-2021)

Chairman: Prof. Francesco Beguinot

PH.D. THESIS

DESIGN STRATEGIES AND ADDITIVE MANUFACTURING OF 3D CUSTOMIZED SCAFFOLDS WITH OPTIMIZED PROPERTIES FOR CRANIOFACIAL TISSUE ENGINEERING

TUTOR

Prof. Vincenzo D'Antò
Prof. Roberto De Santis

PH.D. STUDENT

Dr. Ilaria Onofrio

Contents

Chapter 1: Additive Manufacturing in biomedical applications 1

1.1. Introduction 1
1.2. Additive manufacturing processes: classification 4
1.3. The concept of functionally graded materials 11
1.4. Biocompatible materials and 3D Printing 14
1.5. Improvement of additive manufacturing in the medical field 18
1.6. Bioprinting tissues and organs 19
1.7. Anatomical models for surgical planning 19
1.8. Custom-made implants and prostheses 22
1.9. Tissue engineering approach 23
1.10. Clinical applications in dentistry, traumatology and orthopedics 25
1.11. Benefits of additive manufacturing in medical field 26
1.12. References 29

Chapter 2: Design strategies of 3D customized nanocomposite scaffolds for hard tissue regeneration 31

2.1. Introduction 31
2.2. Materials and Methods 33
2.3. Results and Discussion 36
2.4. Conclusions 47
2.5. References 48

Chapter 3: An engineered design of 3D additive manufactured nanocomposite scaffolds with optimized properties 53

3.1. Introduction 53
3.2. Materials and Methods 54
3.3. Results and Discussion 56
3.4. Conclusions 76
3.5. References 77

Chapter 4: An approach toward the design of 3D customized scaffolds for large cranial defects 81

4.1. Introduction 81
4.2. Materials and Methods 82
4.3. Results and Discussion 83
4.4. Conclusions 84
4.5. References 85

Chapter 1

Additive Manufacturing in biomedical applications

1.1. Introduction

Traditional manufacturing refers to the product manufacturing through subtractive (i.e., machining) or formative (i.e., molds) techniques, characterized by a specific steps sequence and costly infrastructure, with severe limits to the application of timely modifications of the final product [1]. Furthermore, complex geometries often required in biomedical field are difficult to achieve through traditional manufacturing techniques. However, additive manufacturing technique has emerged over the past four decades as a useful tool for cost-effective fabrication of geometrically complex objects in a timely manner [1]. A layer-by-layer deposition of material starting from a computer-generated model represents the basic concept of 3D printing - developed in the 1980s – toward the realization of very complex objects, extremely difficult or even impossible to be fabricated through traditional manufacturing techniques. In this scenario, the role of additive manufacturing becomes extremely important in developing healthcare solutions and in designing implants, as well as in surgical planning, therapeutic delivery and tissue engineering.

On the other hand, *bioprinting* – a rapidly growing application of additive manufacturing - is gaining great interest in research field as it allows for cell seeding in a spatially defined manner in 3D space, thus allowing to produce in vitro models for drug screening and disease modeling as well as *biofabrication* of implantable tissues such as skin, cartilage or bone [1].

Structures characterized by complex shape and geometries should be obtained by means of Additive manufacturing technique in a layer-by-layer fashion starting from 3D model data. Stereo lithography (SLA), Digital Light Processing (DLP), Selective Laser Sintering (SLS), Electron Beam Melting

(EBM), Fusion Deposition Modeling (FDM), Multijet/Polyjet 3D printing, Selective Laser Melting (SLM) and Laminated Object Manufacturing (LOM) etc. can be counted among the Additive Manufacturing techniques. Different kind of materials - ceramics, plastic, metal, liquid, powder or even living cells – should be processed to fabricate any complex 3D component of any shape by utilizing 3D model data [2]. Basically, 3D model data is converted into standard triangulate language format, simply printed by additive manufacturing technique, as shown in Figure 1.1. All of the mentioned techniques - in which the final product is obtained by the layer-by-layer deposition of the selected materials - are based on similar approach. Analogous approach should be translated in the design of healthcare solution, or in obtaining customized complicated anatomical medical structures, starting from 2D radiographic images such as computerized tomography, magnetic resonance images and X-rays to be converted in three-dimensional digital print files [2]. Recent advances evidenced the great potentialities of additive manufacturing in medicine toward a real revolution in healthcare. Fabrication of tissue and organ, anatomical models, development of customized prosthetics and implants, development in pharmaceutical field especially in drug dosage forms, discovery and delivery represent some of the most widely investigated biomedical applications of additive manufacturing. Additive manufacturing is becoming more and more important and extensively adopted in medical field due to the possibility of *customization* and *personalization* of medical products, together with *biocompatibility*, cost effectiveness, improved productivity and accessibility, short production time, simple assembly, collaboration and democratization [2]. Anyway, Additive Manufacturing is still a long way from mass production owing to low speed. However, this latter aspect should be considered at the same time a limitation or a benefit in medical sector, where high precision customized products are required in less quantity. In this context, customized therapy should be adapted with specific changes from one patient to another, making Additive Manufacturing approach and products suitable and most widely adopted in clinical applications [2]. Recently, different researchers and scientists had attempted to map human organs and to convert them into three dimensional virtual designs, successively obtaining vascularized human organs analogues via

Additive Manufacturing and bio-comparable material. However, some regulatory and scientific challenges remain unexplored. 3D medical models should be obtained following distinct fabrication steps: image acquisition, structural target area selection, medical images post-processing toward the evolution in three-dimensional geometry, materials selection, the adequate choice of three-dimensional machine for implant printing together with post processing - if required, testing and final application or implementation in implant body [2]. The proper development of medical model could be useful in enhancing the knowledge and skills of surgeon not only in better understanding diseases, but also in planning costs, surgical processes, application of surgical tools and patient-specific design of implantable devices etc. To this aim, medical additive manufacturing is best suited for custom fit mask, new organ development and operation practice etc. [2-4].

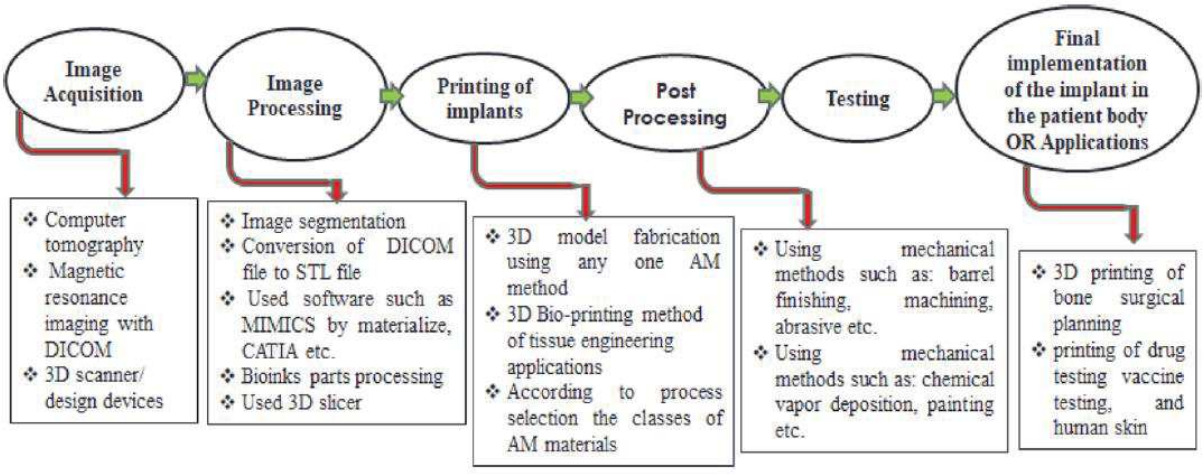

Figure 1.1. Basic steps for the development of 3D printed devices in the medical field [2].

History of additive manufacturing started to 1980s, by Charles Hull. At that time, Hull was working in a Californian manufacturing company that used ultraviolet lamps to add a layer of hard plastic onto surfaces for household applications. He successively proposed to utilize the ultraviolet (UV) light to convert computer aided design (CAD) parts into three dimensional objects, giving life to what will later be called "stereolithography" [2]. After different experimentations, Hull observed that photopolymers (acrylic based substance) exposed to UV light becomes harder. Further, he developed

an apparatus equipped with an ultraviolet light to engrave the acrylic films into shapes and stacked the layers up to finally develop an object. SLA adopted a standard triangulation language file format for data interpretation in a computer aided design file, allowing the electronic communication with three-dimensional printer. After many investigations, he started to write the instruction code for driving the printer to engrave the acrylic layers initially in simple shapes. After eight years (in 1988), he sold the first 3D printer prototype for $100,000 [2]. Later, some companies (Z Corporation, DTM Corporation, Solidscape and Object Geometries) manufactured 3D printers for commercial use. In The first attempts of additive manufacturing applications in medicine (custom prosthetics and dental implants) date back to the 90s. A group of scientists developed an organ starting from patient's cells supported by a three-dimensional printed scaffold [2]. In 2008, scientists developed the first three-dimensional prosthetic leg, whilst in 2012 in Holland, a layer-by-layer three-dimensional printed jaw by a manufacturing company was developed. Thanks to the recent advancements in 3D printing machine and technology, the proposed approach tends to become cheaper and the hospital employment for the realization of human organs analogues became more and more widespread. Additive Manufacturing has altered not only medicine and surgeon approach, but also life expectancy of terminal patients [2].

1.2. Additive manufacturing processes: classification

For each additive manufacturing process, Figure 1.2 reports the most important issues [1].

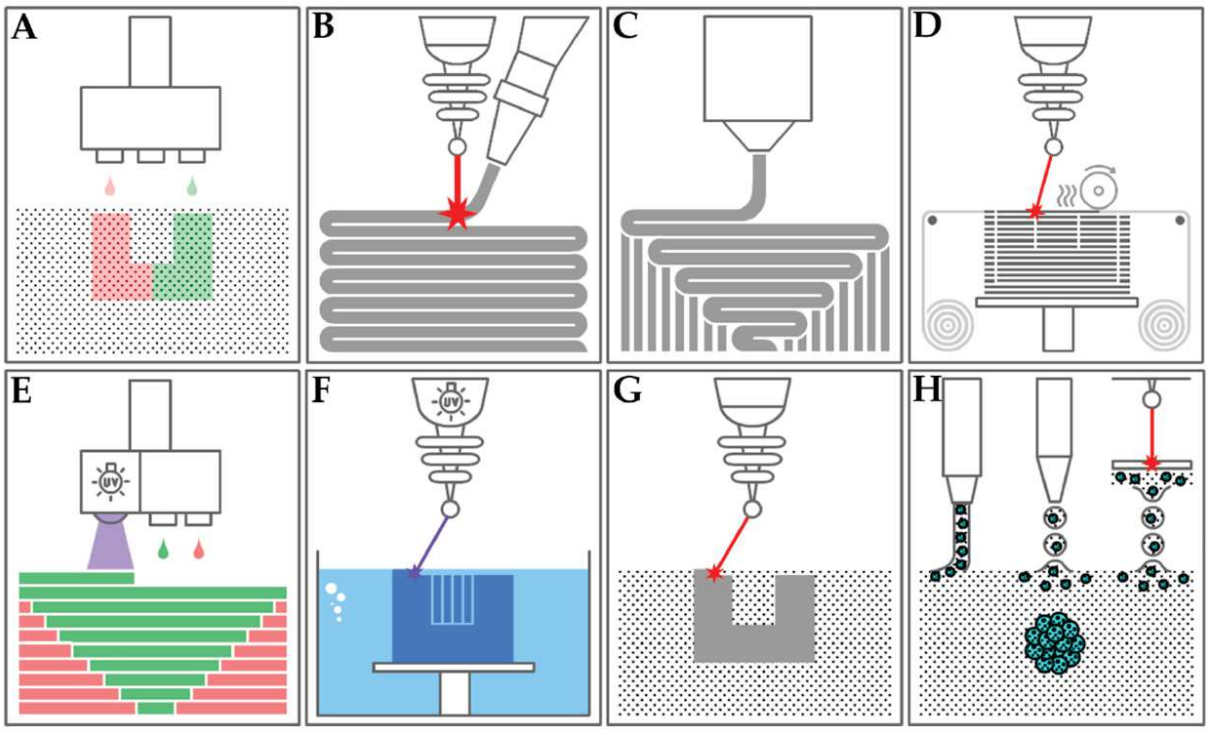

Figure 1.2. Types of additive manufacturing (AM): (A) Binder Jetting; (B) Directed Energy Deposition; (C) Material Extrusion; (D) Sheet Lamination; (E) Material Jetting; (F) Stereolithography; (G) Power Bed Fusion; (H) Bioprinting [1].

- **Vat Photopolymerization processes**. Vat Photopolymerization (VP), tend to produce final parts characterized by high dimensional accuracy and surface finish when compared with many other additive manufacturing processes [3]. Building time represents an advantage of the VP technologies, that are based on mask projection in which an entire part cross section can be projected. VP processes allow to produce final products starting from photopolymers and characterized by worse impact strength and durability than that good quality obtained by injection molded thermoplastics. As a result, mechanical properties of the manufactured parts obtained through VP processes represent the main drawback of the technology [3]. Anyway, the possibility to proper modify the adopted material type together with the optimization of the process, in terms of mechanical properties, can lead to improvements in this field [2-3].

- **Powder bed fusion.** Four different fusion mechanisms should be included in the powder bed fusion (PBF) process group: simultaneous sintering of powder particles with solid-state sintering, chemically induced sintering, liquid-phase sintering, or full melting [3]. In this study, PBF processes will be divided in three subcategories to address the difference in the process mechanism (sintering and full meting) - adopted in the most commercially available apparatuses – and in the energy source (laser or electron beam): selective laser sintering (SLS), selective laser melting (SLM) and electron beam melting (EBM) process groups. PBF additive manufacturing processes, particularly for metal manufacturing, are characterized by high residual stresses lead to the warping of parts [3]. Different approaches have been proposed to minimize this aspect, such as the use of internal cooling channels, the careful selection of the part's orientation and the location of the supports. However, the effects of the part's thermal history (residual stresses and thermal distortions) have to be taken into account. Consequently, the modelling of thermal and thermo-mechanical phenomena taking place in the PBF processes are of crucial importance for the process optimization [3]. Specifically, fusion depth is related to the combination of the laser power, spot size and scan speed whilst the melt pool dimensions have a direct impact on the residual stresses of the parts. The laser absorption characteristics as well as the powder bed density and powder bed thermal conductivity are strongly dependent from powder shape, size and distribution, to be taken into consideration [3]. Moreover, dimensional accuracy, density, shrinkage and curling of the produced part, as well as the recyclability of the unused powder are strongly influenced by the accurate selection of the laser-power and the bed-temperature [3]. Consequently, thermal modelling of those processes must include all the above parameters [2-3].
- **Directed energy deposition**. Simultaneous material deposition and melting are performed in the directed energy deposition processes (DED) [3]. More specifically, energy is guided to a narrow-focused region, where the substrate is melted and heated by the power source (mainly laser beam), while further material is deposited and consequently melted at the same time [3].

The material can either be in wire or powder form. Flexible process parameters' selection characterizes most of the DED machines, although most of them are strongly interrelated (powder feed rate, beam power, and traverse speed) and affect final product features [3]. Furthermore, warping, residual stresses and the surface roughness of the parts are influenced by the melt pool characteristics and the thermal history. On the other hand, droplet kinematics, like in the Material Jetting (MJ – see section below) process group, play a major role here as well [3]. The above references evidenced the importance of modelling of the thermal history of a part, taking into consideration the laser power, scanning speed and melt pool characteristics for the optimization of the process parameters, as well as for the optimization of the process itself, also trying to minimize expensive and time-consuming experimental trial and error methodologies [3]. A plethora of modelling papers on the DMD process already has been exposed to the scientific community and distributed, almost evenly, among the various Key Performance Indicators (KPIs) [3]. More specifically, surface roughness modelling has been presented analytically or numerically. Topology and dimensional accuracy modelling take place in analytical, in analytical-numerical, in numerical, whereas in those issues have been empirically modeled utilizing artificial neural networks (ANN) [3]. Mechanical properties and microstructure modelling has been performed in using analytical, in analytical numerical and in using numerical approaches. Droplet kinematics and flow phenomena have been modeled in using analytical and in using numerical approaches [3]. Finally, heat transfer related KPIs have been modelled either simultaneously with other KPIs (in analytically, in analytically-numerically and in numerically) or exclusively numerically) [3].

- **Binder jetting**. Basically, low strength and stiffness parts are created by means of binder jetting (BJ), with plaster-based powder and water based binder processes [3]. The adoption of infiltrants has been demonstrated to greatly improve material properties. Alternatively, the use of a poly-methyl methacrylate powder and a liquid binder that causes a curing reaction, at room temperature has been also highlighted [3]. In this case however, after completing the

printing process, the part has to remain in the build chamber for several hours for completing the curing process. For metal parts manufacturing via the BJ process, a series of post processes steps are required. More specifically, three furnace cycles are necessary after the printing, for the binder polymer evaporation and for increasing the part's density [3]. This should be achieved by adding extra metal ingots, being in contact with the part. Generally, dimensional accuracy and surface roughness of parts obtained via BJ, are not as good as those made by adopting MJ and they are characterized by poorer accuracies and surface finishes, probably because of the inherent characteristics of the process. Anyway, the improvement of such issues should be pursued by modelling and optimizing the process mechanics [3].

- **Material extrusion**. Fused Deposition Modelling (FDM) represents the commercial name for material extrusion processes. This section aims to analyze some of the major issues that deteriorate the quality of parts obtained via FDM [3]. Part distortions are often attributed to the cooling process profile thus resulting in material warping because of nonlinear cooling. Furthermore, porous parts should be obtained by determining cooling profile. More specifically, the temperature shift between building platform, chamber, and the different layers of the part, play a major role. Additionally, the success of the bonding between layers is strictly linked to the temperatures of the extruder and of the layer on which the filament is placed, playing a crucial role also in mechanical properties of the final part [3,4]. Another important issue is the anisotropic creation of the parts' material properties via material extrusion, due to the crisscrossing extrusion fashion adopted for the filament deposition [3]. Thermal modelling issues concerning the material properties and dimensional accuracy, as well as the improvement of other KPIs, such as building speed and surface roughness, represent the main areas that modelling studies on ME concentrate [3,5].
- **Material jetting**. Different technical problems are related to MJ process. Some of the most important issues are strictly connected to the droplet velocity and size, that strongly influence deposition features [3]. Furthermore, satellite droplets are generated and break off from the

main droplet during the flight, thus resulting in not well-defined boundaries. Primary and "secondary" droplets splashing on impact lead to the formation of a "crown" [3]. All the mentioned issues have to be tackled, in order to improve the quality of parts created by MJ. In this scenario, fluid dynamics should be useful in addressing the most important issues concerned MJ process group, also considering temperature as further parameter. Most of the proposed studies on MJ process group are focused on the droplet kinematics and the flow phenomena [3-8].

- **Sheet lamination**. the bonding of the new sheet on top of the other ones should be pursued through different methods: (a) gluing or adhesive bonding, (b) thermal bonding, (c) clamping, and (d) ultrasonic additive manufacturing [3]. Gluing or adhesive bonding or laminated object manufacturing (LOM) present problems similar to ultrasonic consolidation (UC) process. The bonding efficiency between layers decreases when the laser power induces more thermal energy than it is required. Moreover, part distortions phenomena, due to non-uniform heating and cooling, and edge roughness are frequently observed [3]. Modelling studies to cope with mentioned problems on LOM are based on thermal simulations - analytical and numerical. Voids generated during the fusion of the different layers of sheets between them and hence the reduction of the mechanical features are frequently issued in ultrasonic additive manufacturing or UC [3]. Three different voids categories can be observed: voids generated by (i) surface roughness of two consecutive layers, (ii) damages related to excessive energy input, (iii) defects between adjacent layers [3]. Moreover, anisotropic mechanical properties could be observed because of the differences in the mechanical properties between the interior of the metal foils and the bonding areas where between the different foils. Generally, the anisotropy is greater in the z than it is in the x, y directions. Finally, an important role in the mechanical features of the objects produced by UC is played by local microstructure, considering the possibility that some parts of the foils undergo plastic deformation during the process [3]. Consequently, the research on UC modelling aim to determine process parameters

that will ensure optimized mechanical properties and microstructure, thus minimizing void defects and maximizing linear welding density (defined as the percentage of bonded interface divided by the total length of the interface between two ultrasonically consolidated foils) [3-9].

- **Bioprinting.** Different additive manufacturing technologies to 3D print living cells are included under the definition of bioprinting, not considering as a specific additive manufacturing technique on its own [1]. The deposition of cells suspended in a *bioink* by nozzle-based techniques represents the basic principle, such as material extrusion or jetting, as outlined above, or laser-assisted nozzle-free techniques. Laser-assisted bioprinting involves the transfer of cell-suspended droplets in bioinks, focusing a laser on a membrane coated with cell-bioink on a specific side (the membrane side facing the printing surface) [1]. Reduced shear stress on cells due to an absence of an orifice, and the microscopic resolution are achieved and represent the main advantage of this technique. Inkjet or Drop-On-Demand (DOD) printing may be mentioned as a further technique in which picolitre-volume droplets of cell-containing bioink are deposited with very high precision to coalesce into fibers [1]. The successive crosslinking before subsequent layers deposition ensures 3D structures with sub-100 μm resolution, due to the very small volume of the droplets [1-10].
- **Stereolithography (SLA):** The print bed is lowered into a vat containing a liquid photopolymer resin, and either the resin-bed interface is irradiated by UV or visible light to solidify the resin. The bed containing the polymerized layer is lifted out at every light exposure and dipped back in to repeat the process [1].
- **Nanofabrication**: Structures for various field applications including electronics and medicine characterized by less than 100 nm in size should be processed by means of Nanofabrication, that adopt and employ the same principles of Additive Manufacturing approaches, despite it is not directly recognized as a conventional additive manufacturing technique [1]. The nanofabrication manufacturing process can be divided into two categories [1,11]. A “top-

down" approach that revolves around deconstructing a larger material to form the desired nanostructure, in a fashion similar to that of carving a statue out of a block of stone [1,11]. Complicated and expensive steps are required, with little flexibility for modification. Limited nanostructures reproducibility of the structures obtained through the "top-down" approach can be observed, due to uncontrollable variability in the manufacturing process [1,11]. The "bottom-up" approach represents the second nanofabrication category where building blocks - such as atoms or molecules - self-assemble or are "printed" to create a nanostructure [11], thus leading atomic resolution structures. The "bottom-up" approach is additive in nature, similar to most other additive manufacturing techniques [1]. Endless applications of nanofabrication in biomedicine and tissue engineering are present, including (but not limited to): preserving immunogenicity of compounds in vaccines; minimizing transplant rejection through immuno-isolation; creation of biomaterials with unique mechanical and biological properties; drug sequestration and delivery; and circulating toxin and waste binders [1,11,12]

1.3. The concept of functionally graded materials

Functionally Graded Materials (FGMs) represent materials with changing microstructure, composition and mechanical properties across the volume. In 1984, in Japan was firstly coined the scientific term of functionally graded material [2]. FGM composite materials have been recently considered as novel, smart or advanced quality materials, because of high temperature withstanding, stress intensity factor decreasing and good distribution of residual stresses etc. Furthermore, thermal and mechanical materials properties gradually change from one material layer to another, to fulfil the intended function especially needed for aerospace as well as power industries etc. [2,7]. FGMs were initially adopted as thermal barrier materials for fusion reactors, combustion chamber, turbine blades, space vehicles and aerospace structural applications [2]. Actually, FGMs are considered as potential structural material candidates for aerospace and high-speed automotive applications, also thanks to the excellent resistance against fracture & erosion corrosion (EC), which is the modern requirement

of the industry. The different types of FGMs manufacturing techniques are categorized into distinct groups. The development of FGMs is mainly dependent from adopted process parameters for their manufacturing processes [2]. Among all of the FGMs manufacturing techniques, solid state techniques represent the most promising. In particular, four classes of additive manufacturing processes (Material extrusion; sheet lamination; Powder-bed fusion & Directed-energy deposition) are the most suitable for the purpose. The various additive manufacturing techniques according to their use of production of FGMs are explained in the section below [2].

- **Fused Deposition Modelling (FDM) or material extrusion process**: The FGMs components are produced using fusion deposition modeling and the final properties are directly linked to the adopted process parameters. The lower machine and equipment costs, material flexibility, ease to use, durable and inexpensive raw material represent the main advantages, whereas high surface roughness and prints quality worse when compared to SLA or SLS together with lower mechanical strength are the major drawback of this technology [2]. In this technique the unwound plastic material in semi liquid form is injected through extrusion nozzles tip, onto a base in layers to fabricate a desired component. Lue et al. (2002) used FFF technique to produce a FGMs part. Results revealed that there was a compositional change across the graded sample [2].
- **Powder-bed fusion**: it includes distinct additive manufacturing techniques such as SLM, SLS and EBM. In SLS the laser fuses the powder material, whilst in SLM laser completely melts the powder whereas EBM process requires vacuum for the FGMs components development [2]. Mechanical properties, surface roughness, chemical composition and microstructure of Ti alloy implants manufactured via SLS technique have been investigated by Trainia et al., observing that this process technology is effective for dental implants with functional graded materials manufacturing characterized by superior elastic characteristics very similar to those of the human being bone [2]. Functionally graded scaffold via SLS have been investigated by

Sudarmadji et al., thus proving that SLS is an effective manufacturing method for FGM implants [2].

- **Directed-energy deposition (DED):** FGMs components should be obtained via DED adopting energy in the form of electron beam, laser and plasma arc. In this process either building base is moved while, deposition head remain stationary and viceversa. Laser Metal Deposition (LMD) technique is also dealing with the class of DED method toward the development of functional parts made of FGMs, metal and alloy etc., adopting laser beam of powder/wire material to create a melt pool on the substrate to develop a part in layer-by-layer fashion [2].
- **Sheet Lamination**: Sheet lamination technique was firstly introduced in the market in 1991 by Helist company. Laminated Object Manufacturing (LOM) is an example of this process technology, adopted for FGMs prototypes manufacturing and also considered as economical and fast solid-state technology [2]. This process was invented by Helisys that utilizes sheets of metal or plastic or paper, cut by blade or laser where each sheet showing a slice of CAD model. After the sheets cutting, a binder is used for stacking and bounding purpose and cut sections are removed. FGMs have proven their position among recent advanced materials [2]. They became hard competitors in a wide range of applications starting from the aviation, defense, medical and energy sector. The low cost, process repeatability and reliability represent the future frontiers for functional graded materials. The FGMs biomaterials play an important role in organic systems, providing structural as well as biological functions. Three dimensional reconstructions of human skull defect, skull model, porous Ti implants produced with EBM technique and Ti implant fitted to the skull model are some of the recent advancements in the field of interest [2-3].

1.4. Biocompatible materials and 3D Printing

In the biofabrication field, should be highlighted a clear distinction between direct printing of a cell-seeded material - termed a “bioink”- and the printing of a cell-free scaffold from a “biomaterial ink”, subsequently seeded with cells or directly implanted. Ink selection is driven by both the final function of the part and the printing technique to be used [1]. Biomaterial inks are generally used to produce a solid and rigid scaffold for the permanent or slow-degrading stabilization of a structure, while bioinks produce a softer scaffold more rapidly replaced by the extracellular matrix (ECM) deposition by the embedded cell population [1].

Many bioinks have been developed starting from hydrogels as suitable materials for 3D cell cultures and characterized by very good biocompatibility and highly tunable physical, mechanical and biological properties. Hydrogels commonly show non-Newtonian, shear thinning behavior, which makes them suitable for extrusion bioprinting [1]. If unmodified, however, they often present some important limitations regarding their printing characteristics, well described by Malda et al. Hydrogels are often characterized by low viscosities prior to crosslinking, thus resulting in poor shape fidelity in extrusion-based printing and limiting their capacity to form larger structures without features collapsing. To this aim, in recent years it has been necessary the development of novel bioinks together with the development of new techniques for cell-seeded biofabrication [1]. Biopolymer hydrogels used for bioprinting include, but are not limited to, alginate, agarose, cellulose, collagen, fibrin, gelatin, gellan gum and hyaluronic acid. Alginate is a negatively charged polysaccharide derived from brown algae and is one of the most adopted hydrogels for tissue engineering and bioprinting purposes. It crosslinks upon the addition of divalent cations and can be functionalized by the addition of arginine–glycine–aspartate (RGD) moieties, which are responsible for improved cells binding to the extracellular matrix, facilitating cell-scaffold interactions. Alginate is also frequently blended with other biopolymers to modify both its printing and biological properties [1]. In a recent study hydroxyapatite (HAp) has been incorporated into alginate to produce a bioink for a calcified cartilage matrix production. The addition of HAp into alginate caused a reduction in

glycosaminoglycan (GAG) secretion of chondrocytes, an increase in production of Col II and an increase in calcified cartilage markers Col-X, ALP and Alizarin red staining. More-homogenous distribution of Hap should be pursued by the addition of sodium citrate, thus also improving printing characteristics by preventing clogging of the needle [1]. Gelatin represents another natural biopolymer widely used in cell culture. It undergoes a thermoreversible sol-gel transition if unmodified, but the speed of gelation is generally considered too slow to ensure shape fidelity [1]. Many research groups have used gelatin methacrylate (GelMA) to enable UV crosslinking thus trying to overcome this limitation, also highlighting very good biocompatibility, degradability and a relatively inexpensive GelMA bioink production. A study by Byambaa et al. highlighted that GelMA functionalized with vascular endothelial growth factor (VEGF) moieties should be employed to bioprint spatially defined vascular structures (with HUVECs) within a bone-like (GelMA with silicate nanoparticles and hMSCs) construct. GelMA has also been combined with methacrylated polyvinyl alcohol (PVA-MA) and a visible light photoinitatior to produce a bio-resin for digital light processing (DLP) lithography [1]. This approach allows for freeform fabrication, without the constraints of producing lattices, and with resolution down to 25–50 μm. Human bone marrow derived MSCs was seeded into the bio-resin prior to printing and showed >85% viability 24 h after UV polymerization. GelMA was shown to be an essential addition to PVA-MA for long-term (28 days) cell survival. ECM components, such as collagen, fibrin and gelatin have been widely used to recapitulate the ECM for cell culture scaffolds, but many of the chemical and biological signals from whole ECM are missing [1]. Tissue-derived decellularized ECM (dECM) highlighted the potential to be a very functional bioink; however, the decellularization process often reduces a lot mechanical features, thus requiring the blending with synthetic or natural materials to improve its integrity in the printing process. In a recent study, decellularized dentin was prepared by first removing the pulp and enamel from molars, followed by grinding and decalcification. It was then mixed with sodium alginate and SCAPs to produce a printable bioink [1]. Increasing the concentration of dentin matrix molecules caused a significant increase in the upregulation of dentin markers ALP and RUNX2 [1].

Biomaterial inks often are processed in cytotoxic conditions, i.e. adopting extreme temperature or solvents; however, they can be loaded with therapeutic molecules that can withstand these processing conditions. Thermoplastics, ceramics, composites and metals have all been additively manufactured for use in biomedical applications [1].

Synthetic hydrogels are often not suitable for the direct cell seeding but they show non-Newtonian properties similar to biopolymeric hydrogels, allowing them to be printed by extrusion. Pluronic is a commonly used synthetic ink that can be thermally crosslinked or functionalized with chemical groups for UV crosslinking [1]. Pluronic has been adopted as support material for structures with overhangs, and also as a sacrificial ink to produce hollow structures. Elastomers are also attractive materials for bioprinting because of their mechanical properties that mimic the viscoelasticity of native tissues. Polydimethylsiloxane (PDMS) and silicon have been printed using embedded techniques (freeform reversible embedding (FRE) and printing into microgels, respectively) to produce hollow and bifurcating structures that mimic airways and large vessels. These structures can then be perfused to model flow in large vessels [1].

Thermoplastic materials are also commonly adopted for 3D printing in many technical industries and by hobbyists. In bioprinting, the key advantage is that thermoplastic materials can be processed and undergo multiple thermal cycles for the incorporation of factors, to form filaments for extrusion, resins for photolithography or polymer melts for electrospinning.

Thermoplastics such as polycaprolactone (PCL), polyvinyl alcohol (PVA) and polylactic acid (PLA) have been bioprinted for use as both supports for cell-seeded hydrogels that require mechanical reinforcement, and for direct implantation in vivo. They are printed using extrusion from filaments or polymer melts so they can produce high resolution structures with very good shape fidelity, excellent control over porosity, which can in turn influence the mechanical properties of the scaffold [1].

Ceramic materials are characterized by a mixture of inorganic salts, including calcium and phosphate, mainly adopted for bone and dental applications for their osteoconductive features. Ceramics are very

brittle making difficult to handle and implant. In biofabrication approach, ceramics are often combined with a polymeric binder for extrusion bioprinting or 3D powder printing. Commonly printed ceramics include tricalcium phosphate (TCP), hydroxyapatite (HAp), bi-phasic calcium phosphate (BCP), poly (methyl methacrylate) (PMMA) and bioglass. Tetracalcium phosphate (TTCP) represents also a promising candidate for bone replacement and has been shown to be highly resorbable at low pH [1]. In a study by Mandal et al. TTCP with a phytic acid binder has been analyzed. Following the printing and post-hardening with additional binder solution, TTCP was still the most abundant ceramic phase, but an amorphous calcium phosphate phase can be observed, indicating a reaction between the ceramic powder and binder [1]. Multi-layered scaffolds have been also obtained by combining and PCL via mixing the powdered ceramic and polymer and producing a liquid melt successively extruded. PCL blended with natural ceramics (decellularized bone matrix and Bio-Oss, a bovine derived bone mineral) outperformed synthetic ceramics (HAp and TCP) regarding osteoinductive capability [1].

On the other hand, metallic implants for orthopedic, dental and craniofacial applications have traditionally been fabricated by methods such as casting, forging and machining starting from stainless steel, cobalt chromium molybdenum and titanium alloys. Patient-specific implants have been developed by means of additive manufacturing technology benefiting from reconstructed 3D imaging data. Recent advancements regard the possibility to add tunable functionalities to these implants [1]. A recent study showed how it is possible to load an antibiotic-eluting cement into a central cavity of an innovative metallic implant that could not be manufactured by conventional methods. High resolution achievable by selective laser melting (SLM) of metallic powders allows to produce intricate lattices, thus overcoming issues surrounding stress shielding in hip implants. Finite element analysis (FEA) should support for the determination of theoretical mechanical performance and theoretical reductions in bone loss of porous implants obtained via SLM, also confirming FEA prediction by mechanical testing [1].

1.5. Improvement of additive manufacturing in medical field

Different additive manufacturing processes have been adopted by researcher in distinct areas of medical field [2]. According to the American Professional Association Report, the additive manufacturing is estimated to rise by $9.7 billion by 2027 in dental application (increasing 35% annually). The use of 3D printing is also growing day by day especially in medical field. About 11% of medical industries revenue comes from three dimensional printed components, whether medical device or implants. The growing need of additive manufacturing is due to requirements of customize medical parts [2,10]. According to the web of science data, total 1157 research papers of additive manufacturing for biomedical applications has been published from 2011 to Oct, 2020. Several kind of materials potentially usable for 3D printing medical applications have been shown. The selection of material mainly depends on the utility/properties required in the final part production or additive manufacturing model such as customized implants, surgical tools, prosthetic limbs, tissue scaffolds etc. Strength, durability and flexibility represent key features for medical applications where acrylonitrile butadiene styrene (ABS) and nylon represent a good choice [2]. However, polylactic acid (PLA) is a suitable biodegradable material for biomedical applications. An ideal biomaterial should possess different peculiar characteristics. It should be easy to print, biocompatible, morphologically mimic living tissue, nontoxic etc. Metal and alloys are used where high strength parts are required – i.e. in orthopedic implants, plates, screw etc. Ceramic materials are suitable for bioactive orthopedic implants, whilst composites for porous orthopedic implants with better mechanical properties have been widely investigated. However, among all biomaterial, polymer-based materials are widely used in biomedicine (86%) [2]. Anyway, the material selection for the specific biomedical applications depends upon specific implant requirements. Biomimetic materials are also required for tissue engineering applications. The designing enhancement of scaffolds through conventional method (Salt leaching & Phase separation) has been performed by different research groups, adopting distinct process methods such as rapid prototyping (RP), electrospinning etc. for three-dimensional biomimetic scaffolds manufacturing. Bone tissue engineering plays important role

in the damaged tissues and harvested treatment. The ceramics as well as polymers such as polycaprolactone and poly (lactic co-glycolic) acid are extensively adopted in bone tissue engineering. Various additive manufacturing methods have been analyzed using *in vitro* testing for biomedical applications such as medical education, surgical planning etc. [2].

1.6. Bioprinting tissues and organs

Artificial living tissues should be developed via bioprinting process and computer-guided pipette to living cells (bio-ink) layer on top of one another. Bioprinting is used to fulfill the requirements for living organs and tissues suitable for tissues transplantation and regeneration - such as heart tissue, bone, tracheal splints, cartilaginous structures, vascular grafts and multilayered skin etc. These artificial tissue organoids or constructs can be utilized for medical research purposes as they mimic organs on a miniature scale. Recently, it has been proposed a bioprinting classification into 3 distinct types: laser based, Inkjet or Drop-On-Demand printing technology [2].

1.7. Anatomical models for surgical planning

Additive manufacturing is based on post-processing and converting 2D (MRI or CT scans) into 3D images thus supporting surgeons in better planning and surgical training, also creating patient-specific implant organ models that surgeons can utilize to practice on before conducting any complicated surgeries. Most widely used anatomical models have been proposed in maxillofacial, orthopedics and neurological surgery [2]. In vitro applications of tissue engineering have paved the way for the development of physiological models representing tissue-like human and animal microenvironments for more clinically applicable testing [1]. Complex three-dimensional organizations of different cell types allow for the organoids creation [1]. Furthermore, functional units of different organs should be useful for studying disease processes and treatment responses. It has also been shown that cells behave quite differently in terms of gene expression and signaling within a 3D environment, as opposed to conventional 2D cultures. Riedl et al. in a study compared the response of 3D spheroids

vs 2D cultures of human colon cancer cells lines, observing contradictory levels of AKT/mTOR/S6K signaling activity upon treatment with the mTOR inhibitor rapamycin. Signaling pathways was increased in 2D cultures but decreased in 3D spheroids [1]. In a xenografted mouse tumor model, it has been demonstrated that the 3D spheroid model was an accurate representation of the in vivo response to rapamycin treatment, showcasing the increased efficacy of 3D spheroids as accurate preclinical drug screening models compared to 2D cultures [1]. Tumor spheroid models recreate in vivo-like environments in a relatively inexpensive and fast way, but they are limited regarding size and complexity and the nutrients, gases and wastes diffusion. Spheroids can only grow to a certain size before hypoxia and lack of nutrients [1]. Additionally, fabrication methods for spheroid formation only allow for production of simple spheroids, without any design complexity, and they are also very fragile during handling. As an additive manufacturing technique, bioprinting allows the creation of complex 3D hydrogel models with great levels of control and reproducibility compared with conventional techniques such as molding and spheroid formation [1].

Bioprinting can already allow the creation of complex organ-on-a-chip models, with good anatomical, compositional, and functional similarity to the host tissue, the aim being to conduct experiments in an in vivo-like physiological environment [1]. Organ development begins in the embryonic period. Recreating architectural environment and correct signaling patterns, the modeling of both developmental and disease processes should be pursued. Current research efforts have been successful in reproducing functions of many different organs through differentiation and self-organization of stem cells into organoids. Reliance on the self-organizing capabilities of stem cells, however, provides limited control regarding the shape, composition and final size of the organoid. Stem cells, cell lines or patient-derived cells can be deposited with good spatial control to achieve any desired structural arrangement through bioprinting [1]. A study by Grix et al. utilized stereolithography to produce 4 mm 3D liver lobule models. Hepatocyte-seeded GelMA (methacrylated gelatin) with degradable PEG (polyethylene glycol)-lined channels have been proved to mimic the unique in vivo architecture of the liver, also demonstrating increased hepatocyte-specific

gene expression within the 3D model if compared to 2D monolayer cultures. Additionally, a vascular network for perfuse the model should be obtained by embedding channels [1]. The high resolution offered by stereolithography technology allowed printing of microscopic details. Another study by Material extrusion bioprinting of a collagen-based bioink has been proposed by Bulanova et al. to create a vascularized thyroid gland model to create a model consisting of embryonicstem-cell-derived thyroid spheroids and epithelial spheroids, in close proximity to each other, that allowed for invasion and vascularization of the thyroid spheroids by the epithelial cells [1]. They also confirmed the functionality and neovascularization of the organoid by achieving thyroid homeostasis after implanting the bioprinted organoid in hypothyroid mice. Over the past few years, highly complex organoids and lab models have been proposed to be obtained via emerging bioprinting. To date, many labs have utilized this technique for creating biologically functioning models made up of a wide variety of tissues such as liver, mammary epithelium, myocardium, skeletal muscle, kidney, skin, neurons and malignant tumors [1].

These models are becoming useful drug screening tools within both research labs and the pharmaceutical industry.

There are, however, few limitations associated with bioprinting. The properties of currently adopted bioinks result in a trade-off between creating a viable growth environment for cells, while providing structural support to the printed model. More elastic biomaterials can allow for creation of complex models that can hold their shape but at the same time limit cellular interactions and movement [1].

More viscous biomaterials create a fluid environment for cells, while having less capability to create large models without collapsing under their own weight. As the field of bioprinting advances, so does the need for discovering new biomaterials that provide structural support without hindering cell viability and extracellular matrix deposition [1].

1.8. Custom-made implants and prostheses

3D printing technologies are also adopted to develop customized prosthetic limbs to suit and fit the wearer. It speeds up the process in economical products manufacturing providing patients the same functionality as product obtained via conventional methods [2]. 3D printing represents a very effective approach in producing customized implants and prostheses and it solves many orthopedics problems. The custom-made maxillofacial implants, cranial implants, mandible implants, and orthopedics implants etc. have been widely explored. Additionally, 3D printing advances are related to scaffoldings and tissue engineering, mechanical bone replicas, forensics, surgical planning, design of medical instrument and customized implant design [2].

The field of surgical implants and prostheses is continuously developing to allow for more cohesive integration of these foreign objects within their surrounding tissue, as well as to increase their functionality [1].

Design of implants and prostheses requires a multidisciplinary approach that combines principles of materials science, engineering, biomechanics, molecular biology, pharmaceuticals and long-term clinical monitoring.

Additive manufacturing can help to bridge the gap between biology and engineering by creating complex biocompatible and bioactive constructs that take advantage of unique material properties, such as osteoconductivity and osteoinductivity, to promote tissue regeneration and integration of the implant with the surrounding tissue [1].

Current radiological imaging technology, such as computed tomography (CT), can allow for creation of very accurate CAD models of a defect that can serve as models for 3D printing to ensure a perfect fit into the desired tissue [1].

1.9. Tissue engineering approach

Tissue engineering plays a pivotal role in the fabrication of biocompatible implants to replace damaged or non-functional tissues by combining biocompatible materials, live cells and growth factors to create implants that aid normal tissue growth throughout the engineered construct [13-15]. Additive manufacturing finds wide acceptance in tissue engineering applications, allowing for the fabrication of 3D-printed models that mimic the microscopic network of connective tissue [1,13]. From porous implants that promote bone regeneration, to complex three-dimensional organoids composed of cells [1,15,16], the main advantage of 3D printing in tissue engineering is the ability it provides to make geometrically complex (potentially composite) structures by accurate placement of material or cells within a three-dimensional space [1].

Bone defects, injuries, harmful diseases, accidents should damage human tissues thus provoking the loss in the working of joints and organs. To restore the functions of injured joints, a surgery is usually needed [2]. Tissue engineering adopts different techniques (gas foaming, freeze-drying, electro-spinning, solvent casting, emulsification) to manufacture scaffolds for potential application in damaged tissues. As key features, low cost, customization and personalization of medical parts, improved collaboration, democratization of design and fabrication etc. are some of the main advantages of 3D printing approach in biomedicine. Several kinds of biomaterials should be employed for different applications of tissue engineering in 3D printing technology in bone, skin, nerve, vascular, and cardiovascular, meniscus, urethra regeneration, and so on [2].

Effective implant production for bone regeneration in vitro and in vivo should be obtained by AM approaches, thus intervening in the management of critical-size bone defects, often resulting in significant morbidity [1]. Just as an example, a large bone defect should be simply filled with bone graft, but bone integration should not be guaranteed due to an absent coherent blood supply to the graft [1]. Current surgical management options include vascularization of a bone graft, which is difficult to achieve, or performing a Masquelet procedure, effective in restoring blood supply, but requires multiple operations thus increasing morbidity [1]. Additive manufacturing offers potential

implant solutions for both vascularization and bone regeneration improvements. Porosity represents an important property for promotion of bone ingrowth. 3D printing provides the technical capability to create high-resolution, porous scaffolds from a wide variety of materials including metals, ceramics and biodegradable polymers. Other regenerative capabilities of additive manufactured scaffolds aside from bone have also been studied. A study by Lee et al. demonstrated that the printing and implantation of an acellular hydroxyapatite/PCL scaffold doped with transforming growth factor -3 (TGF-3) into rabbits resulted in full regrowth of the articular surface of the proximal humeral joint [1], and the regenerated cartilage had comparable histological, compressive and shear properties to that of native rabbit articular cartilage. Similar findings were observed by Chang et al for an FDM-printed PCL trachea, coated with MSCs and fibrin, demonstrating neocartilage production and integration with native tracheal tissue [1]. Tissue regeneration using FDM-printed scaffolds have also been reported with hydroxyapatite–PCL scaffolds in the periodontium. The initial physical interaction of implants with surrounding tissue occurs at the implant surface, thus suggesting important findings in the study of implant failure over time [1]. In particular, it is important to analyze the stress shielding due to differences in mechanical properties (compared with the surrounding tissue) and implant wear-induced cell death from movement across the implant-tissue interface. Implant surface characteristics should be optimized for maximize the integration and fixation to the surrounding tissue. In this scenario, surface roughness of metallic bone implants is an important factor that inversely correlates with biological fixation to the surrounding bone. A study by MacBarb et al. demonstrated that 3D-printed titanium spinal implants obtained via Electron Beam Melting (EBM) were superior for inducing osteoblast proliferation and calcium production on implant surface *in vitro* if compared to the current standard of implant surface processing (titanium plasma spraying). Cancellous bone-like trabecular network incorporation on the implant surface 3D model has been pursued and subsequently high-resolution fabrication using additive manufacturing has been provided [1]. Porous coatings for 3D-printed implants via nanofabrication techniques have also been used analyzed. A study by Garcia et al. showcased how by fibronectin nanoclusters coating on titanium

implants resulted in a significant increase in integrin binding, resulting in improved implant fixation in rats. Selenium nanoclusters coated titanium implants have been also proposed in another study by Tran et al. in an *in vitro* model, resulting in enhanced antitumor activity, while also promoting healthy bone formation on the bone surface compared to untreated implants [1].

1.10. Clinical applications in dentistry, traumatology and orthopedics

Dentistry, in particular in the two branches relating to oral and maxillofacial surgery, orthogenetic, endodontic and orthodontic etc. represent the field of major investigation of medical additive manufacturing [2]. High quality restoration as well as comfort to dentists should be achieved. In addition, dental restorations, which are being created through additive manufacturing, are more robust in production than restorations created by dental technicians. Various additive manufacturing techniques (FDM, SLS, LOM) are used to print dental pieces and produces bridges, orthodontic appliances, crowns etc. In addition, AM in oral surgery represents a novel approach in helping surgeon simulation/planning and in providing overview to surgeon before starting the patient surgery [2]. A customized approach adoption for the management of each patient became necessary because of anatomical variability in dentistry. Recent advancements in scanning and imaging technologies have resulted in highly accurate 3D reconstructions of the oral cavity to serve as a template for designing custom oral prostheses and implants. In the field of prosthodontics (dentures), additive manufacturing is clinically established as a feasible and accurate approach for fabricating prostheses with comparable durability to conventional manufacturing techniques and materials [1]. Stereolithography is a commonly adopted technique in this field, with established commercial resin products available. In orthodontics (retainers), CAD models of a patient's oral cavity and teeth are used to simulate the final teeth-alignment goal, and to print a corresponding mold for fabricating custom silicon prostheses. In oral and maxillofacial surgery, a major role of additive manufacturing is in 3D printing custom biocompatible and osteoinductive implants to accurately fill bone defects and promote regeneration of the bone [1].

It is the first medical sector to adopt additive manufacturing method to manufacture patient specific models, also for maxillofacial surgery [2]. Furthermore, additive manufacturing produced models and plays an important role mainly for surgeon training, surgical planning and decreasing the re-operation rate in orthopedics, in particular regarding joint arthroplasty, trauma surgery, deformity improvement etc. The major applications in traumatology and orthopedics include surgical guides, biomaterials, implant, orthoses, traumatology, etc. [2].

1.11. Benefits of additive manufacturing in the medical field

The word personalization means to fulfill the customer's demand efficiently and effectively and making interactions easier and faster, hence increasing customer-satisfaction. Customization is related to the action of modifying something to suit/fulfil a particular individual or task. Custom-made implants, surgical tools and fixtures can have a major effect in terms of time needed for surgery, patient recovery time. Additive manufacturing is able to cost-effectively produce product/items [2]. In this context, costs of 3D printing decreases for small dimension implants or prostheses such as those used for dental and craniofacial disorders. In addition, additive manufacturing also decreases the fabricating costs by decreasing the application of unnecessary resources. Some drug may also be printing in dosage form that is easier and highly cost effective to deliver to patients [2]. 3D printing technology became faster as compared to traditional techniques of producing products like prosthetics and implants, based on processes such as forging, milling and a very long delivery time. In addition, speed, reliability, and resolution of additive manufacturing method are also related to the rising availability of materials [2]. Finally, costs reduction allows more people to use little more than a 3D printing machine and their imaginations to design and produce novel products for commercial and personal use. The medical model fabricated by 3D printing technology possess higher accuracy and surface finish. Furthermore, accurate selection of the material to enhance different features of medical implant could be pursued taking into account fast and easy to use 3D printing approach [2]. No tooling or fixture is required. The word "mass customization" was firstly raised by Davis in 1980s suggesting

the ability to produce functional parts that meet the individual customer satisfaction and needs with reasonable cost. Embedded customization, modular production, and customized product services are the major stages of mass customization that become a dominant product manufacturing strategy. Obviously, compulsory quick changes for product manufacturing companies in the view of vast competition, globalization, rapid technological innovations etc. became evident [2]. Additive manufacturing is cost-effective only if the part is produced for specific need/customer satisfaction otherwise it is highly expensive and lot of wastage. Customization help to miniature batch sizes and need frequent as well as dynamic re-configuration of the manufacturing system. The accurate selection of material for medical implant manufacturing is mainly guided by bio functionality, biocompatibility, resistance against corrosion etc. Metallic biomaterials are often used to replace or support skeleton portion. If we compare metallic with ceramic and polymeric materials, high fracture toughness, tensile properties and fatigue strength should be highlighted [2]. The cobalt alloy possesses many attractive properties such as resistance against wear, corrosion resistance, heat resistant etc. But the limitation of cobalt alloys is the very cumbersome to manufacture, therefore its applications has been limited. Although additive manufacturing has lot of advantages (innovation, creation of complex shape, less waste, cheaper for small batch production, single step operation, less wait age time, customization and high flexibility) over traditional manufacturing, it still presents some limitations (poor mechanical properties and limited materials availability, high cost for large volume production etc.) [2]. To this aim, it is widely recommended to mention a comparison between additive manufacturing and conventional manufacturing processes also in order to address future research in overcoming the challenges of additive manufacturing processes. Additive manufacturing is an effective, novel, revolutionizing and rapidly growing technology especially in medical sector. Recently, additive manufacturing technology provided a large opportunity to help pharmaceutical and medical companies to generate more specific drugs and changing the way that surgeons and doctors plan procedures, toward a customization with high accuracy [2]. The four major core applications of additive manufacturing in medical field that are associated with recent innovations

are: bioprinting tissues and organoids, patient-specific surgical models, surgical tools, and custom-made prosthesis. Recently, additive manufacturing providing distinct possibilities for application in medicine such as in craniofacial implants to hip, knee and spinal implants, prosthetic dentistry, production of various medical tools used for cutting and drilling in surgery etc. A comprehensive literature review has been performed to study the mechanical properties of different additive manufacturing processes with different materials and their biomedical applications [2]. Some more applications such as organ printing is still needed to be investigated. Additive manufacturing provides number of advantages to manufacturers such as cost savings and optimization of product design, shorter supply chain, customization, ability to produce complex geometry, etc. Over the last decade, additive manufacturing growing rapidly in the medical sector, however, there are still some challenges in adopting 3D printing. Some important challenges for the manufacturer are reported below [2]:

- Limited choice of materials: The raw materials source for the fabrication of suitable or similar part/object to human organs and tissues are limited.
- Poor mechanical properties: The part should have reasonable mechanical characteristics such as compress strength, tensile etc. after printing process.
- Low dimensional accuracy: The component fitting is very essential for a highly precise design; the barrier is to overcome the shrinkage of the component during the process of cooling.
- Customization of fit & design: As the part is fabricated to the patient function, shape or size, it cannot be utilized in other patients. In addition, the other challenges of additive manufacturing include high cost of printer, not suitable for mass production, post-processing requirements, speed of bioprinter. Hence more research is required on 3D printing material, process technique and applications of additive manufacturing [2].

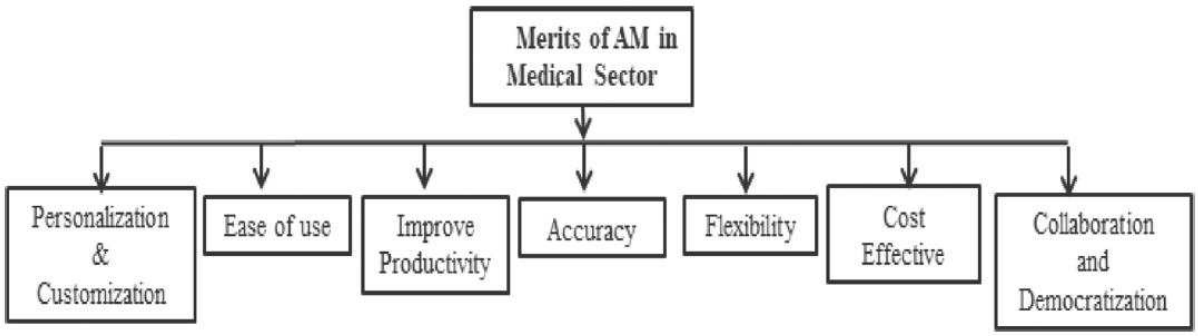

Figure 1.3. Merits of additive manufacturing in medical applications [2].

1.12. References

[1] Pouyan Ahangar, Megan E Cooke, Michael H Weber and Derek H Rosenzweig. Current Biomedical Applications of 3D Printing and Additive Manufacturing. Appl. Sci. 2019, 9, 1713.

[2] Rakesh Kumar, Manoj Kumar c, Jasgurpreet Singh Chohan. The role of additive manufacturing for biomedical applications: A critical review. Journal of Manufacturing Processes 64 (2021) 828–850.

[3] Panagiotis Stavropoulos* and Panagis Foteinopoulos. Modelling of additive manufacturing processes: a review and classification. Manufacturing Rev. 5, 2 (2018)

[4] Gibson, D. Rosen, B. Stucker, Additive manufacturing technologies: 3D printing, rapid prototyping, and direct digital manufacturing, Springer, Berlin, 2014.

[5] S.H. Ahn, M. Montero, D. Odell, S. Roundy, P.K. Wright, Anisotropic material properties of fused deposition modelling ABSRapid Prototy. J. 8 (2002) 248–257.

[6] M. Bussmann, S. Chandra, J. Mostaghimi, Physics of Fluids 12 (2000) 3121–3132.

[7] Pradhan P, Kumar S, Pattnaik S. A state of the art in functionally graded materials and their analysis. Mater Today Proc 2009;18:3931–6. https://doi.org/10.1016/j. matpr.2019.07.333.

[8] Kumar S, Kumar M, Handa A. Combating hot corrosion of boiler tubes- a study. Eng Fail Anal J 2018; 94: 379–95. https://doi.org/10.1016/j. engfailanal.2018.08.004

[9] Suresh S, Mortensen A. Functionally graded metals and metal ceramic composites: part 2 Thermomechanical behaviour. Int Mater Rev 1997; 42:85–101.

[10] Javaid M, Haleem A. Additive manufacturing applications in medical cases: a literature based review. Alexandria J Med 2018; 54:411–22.

[11] Biswas, A.; Bayer, I.S.; Biris, A.S.;Wang, T.; Dervishi, E.; Faupel, F. Advances in top-down and bottom-up surface nanofabrication: Techniques, applications & future prospects. Adv. Colloid Interface Sci. 2012, 170, 2–27.

[12] Ruiz-Hitzky, E.; Aranda, P.; Darder, M.; Ogawa, M. Hybrid and biohybrid silicate based materials: Molecular vs. block-assembling bottom-up processes. Chem. Soc. Rev. 2011, 40, 801–828.

[13] Chocholata, P.; Kulda, V.; Babuska, V. Fabrication of Sca_olds for Bone-Tissue Regeneration. Materials 2019, 12, 568.

[14] Zhu, L.Y.; Li, L.; Shi, J.P.; Li, Z.A.; Yang, J.Q. Mechanical characterization of 3D printed multi-morphology porous Ti6Al4V sca_olds based on triply periodic minimal surface architectures. Am. J. Transl. Res. 2018, 10, 3443–3454.

[15] Ma, Y.; Hu, N.; Liu, J.; Zhai, X.;Wu, M.; Hu, C.; Li, L.; Lai, Y.; Pan, H.; Lu,W.W.; et al. Three-Dimensional Printing of Biodegradable Piperazine-Based Polyurethane-Urea Scaffolds with Enhanced Osteogenesis for Bone Regeneration. ACS Appl. Mater. Interfaces 2019, 11, 9.

Chapter 2

Design strategies of 3D customized nanocomposite scaffolds for hard tissue regeneration

2.1. Introduction

Bone is capable of healing and remodeling itself except in the case of defects that exceed a critical size [1,2]. Autografts are generally considered the gold standard for bone reconstruction. Even though it is reported that there is no risk of device rejection or disease transmission, many complications arise due to poor availability, prolonged hospitalisation, donor-site morbidity and pain, and high risk of infection and haematoma [1-3]. For this reason, allografts may be seen as an alternative to autografts but their clinical applications are strongly limited by the risk of pathogenic disease transmission as well as low integration with native tissues [2,4-9]. The use of metallic or ceramic man-made devices may be considered to be an interesting alternative system since these devices can immediately act as a mechanical support, providing the structural stability that is generally needed for the bone healing process. However, the use of metallic devices may lead to the risk of bone resorption and fracture as a consequence of the low torsion of the great mismatch between the mechanical properties of the implant and the bone. Alternatively, the brittleness of ceramic devices with high osteointegration and osteoinduction properties clearly limits their use [2,4,9-16]. Thus, for many years, novel approaches based on the combination of scaffolds with cells and/or biomolecules have been gaining importance as an intriguing strategy with which to overcome the above reported drawbacks [16]. The great challenge should be the design of a suitable biomechanical environment

for cell growth and the consequent new tissue formation. Over previous years, different combinations of scaffold design strategies, materials, biomolecules, and cells have been widely investigated in an attempt to promote an effective interaction with the native tissue [2,17,18]. In the field of tissue engineering, poly(ε-caprolactone) (PCL), which is an aliphatic polyester, represents one of the most commonly used biodegradable polymers, due to its interesting processability, biodegradation rate, and high thermal and chemical stability [2,19-21]. The development of ceramic materials with a composition similar to the bone mineral phase, such as hydroxyapatite (HA) and tricalcium phosphate, has potentially led to the possibility of improving both the bioactivity and the mechanical properties of the neat polymeric scaffolds [22-24]. With regard to bone tissue regeneration, PCL/HA nanocomposite scaffolds with tailored architectures and mechanical and mass transport properties have already been fabricated by additive manufacturing techniques (i.e., fused deposition modeling/3D fiber deposition) that allow the development of customized structures as well as the control of pore geometry and spatial distribution [16]. Nevertheless, it is well known that the process and instrument parameters play an important role in determining the mechanical properties and morphological features of additively manufactured scaffolds. In this context, the influence of the process parameters on these characteristics has previously been studied in the case of 3D additively manufactured PCL scaffolds obtained through a bioextruder [25]. In particular, great efforts were devoted to the study of the effect of the deposition velocity (DV), screw rotation velocity (SRV), slice thickness (ST), and process temperature (PT) to find the best set of parameters for the fabrication of PCL scaffolds with enhanced properties and reproducibility [25]. In the processing of nanocomposite materials, the difficulties are usually greater than those encountered for the neat polymers. Accordingly, taking into account the previously obtained results for the neat PCL structures [25], in this study, an optimisation design strategy for additive manufacturing processes based on extrusion/injection methods was first employed to develop PCL/HA nanocomposite scaffolds for hard tissue regeneration. The nanocomposite scaffolds were analyzed at different levels, and examples of strategies for the development of customized scaffolds were reported.

2.2. Materials and Methods

PCL/HA nanocomposite pellets were first developed and then processed through the fused deposition modeling (FDM)/3D fiber deposition technique. Specifically, PCL (Mw = 65000; Sigma-Aldrich, St. Louis, MO) pellets were dissolved in tetrahydrofuran (THF; Sigma-Aldrich, St. Louis, MO) while stirring at room temperature. HA nanoparticles and ethanol were then added to the solution. A PCL/HA weight ratio (w/w) of 90/10 was considered, and an ultrasonic bath (Branson 1510 MT, Danbury, CT) was employed for the dispersion of the nanoparticles in the PCL/THF solution. PCL/HA nanocomposite pellets were processed using a bioextruder [2,25] to fabricate 3D scaffolds (length L_0 of 7.0 mm, width W_0 of 7.0 mm, and height H_0 of 8.0 mm), characterised by a 0/90° lay-down pattern. A nozzle with an inner diameter of 400 μm was used to extrude/inject the material. The nanocomposite fibers/filaments were deposited according to the selected sequence of stacking (i.e., lay-down pattern). A fiber spacing (i.e., filament distance [FD]) of 1,000 μm was used.

The PCL/HA scaffolds were manufactured using three different values of the ST, DV, SRV, and PT, as shown in Table 2.1 [2].

ST (μm)	DV (mm/s)	SRV (rpm)	PT (°C)
350	8	20	120
380	10	25	130
400	12	30	140

Table 2.1. Manufacturing parameters: slice thickness (ST), deposition velocity (DV), screw rotation velocity (SRV) and process temperature (PT).

With regard to the fabrication of the devices, one parameter was varied iteratively, while maintaining the other three as constant parameters. The morphology of the scaffolds was investigated by scanning

electron microscopy, focusing on the filament diameter, strand distance (center-to-center distance), and layer thickness. The mechanical behavior of the 3D scaffolds was appropriately analyzed. Compression tests on the 3D scaffolds and nanoindentation analyses on the scaffold fibers were performed to assess the effect of the inclusion of HA nanoparticles on the mechanical behavior and local surface properties. In particular, mechanical compression tests were carried out on the fabricated 3D PCL/HA scaffolds. The structures were tested at a cross-head speed of 1 mm/min up to a strain of 0.4 mm/mm, using an INSTRON 5566 testing system.

The "apparent" stress (σ) and strain (ε) were calculated as reported below [2,16,25]:

$$\sigma = \frac{F}{L_0 \cdot W_0} \qquad (2.1)$$

$$\varepsilon = \frac{\Delta H}{H_0} \qquad (2.2)$$

with F representing the force measured by the load cell, whereas ΔH represents the height variation of the device.

The slope of the initial linear portion of the stress–strain curve was considered to determine the compressive modulus [2]. For each set of parameters (Table 2.1), five specimens were mechanically tested.

Nanoindentation analyses were performed using the Nanotest Platform (Micromaterials, U.K.) in a specific load range (1–5 mN). A diamond pyramid-shaped Berkovich-type indenter tip was employed. The trapezoidal load functions characterised by the specific values for the load hold periods (i.e., 20 s) and the

loading–unloading rates (i.e., 300 μN/s) were considered. Using the Oliver and Pharr method, the hardness values were evaluated from the load-depth curves.

The hardness (H) was calculated as follows:

$$H = \frac{L_{max}}{A_c} \quad (2.3)$$

where A_c and L_{max} are the projected contact area and the applied peak load, respectively. The biological performances of the fabricated PCL/HA scaffolds were assessed to analyse the effect of the nanoparticle inclusion. Briefly, PCL/HA scaffolds were prepared for cell seeding following a reported protocol [2,16]. PCL and PCL/HA scaffolds were seeded with bone marrow-derived human mesenchymal stem cells (hMSCs) using 1×10^4 cells/sample. The cell viability was evaluated at different time points using the Alamar Blue assay (AbD Serotec Ltd,UK). The cell adhesion and spreading were analyzed at different time points using confocal laser scanning microscopy (CLSM) and rhodamine phalloidin staining. The Image J software was employed, and a shape factor was introduced to analyse the CLSM images of the cell-scaffold constructs [23]. The shape factor was calculated as follows:

$$\phi = \frac{4\pi A}{P^2} \quad (2.4)$$

with A and P representing the area of a cell and the perimeter, respectively. Considering that circular objects are characterised by the greatest area-to-perimeter ratio, a shape factor of 1 represents a perfect circle. Thin thread-like objects have the lowest shape factor, which approaches zero [2,23].

The cell-scaffold constructs were also incubated in lysis buffer and centrifuged. The alkaline phosphatase (ALP) activity was measured using the SensoLyte pNPP alkaline phosphatase assay kit (AnaSpec Inc., Fremont, CA, USA). DNA was also detected and quantified by the Quant-iT PicoGreen assay kit (Molecular Probes Inc., Eugene, OR, USA). The normalized ALP activity (ALP/DNA) was determined. The experiments were performed at least three times in triplicate.

An example of the design and production process of customized PCL/HA nanocomposite scaffolds for mandibular defect regeneration (i.e., symphysis and ramus) was also reported, integrating

different methodologies and approaches (material synthesis/preparation, reverse engineering, and additive manufacturing), as seen in Figure 2.1 [2].

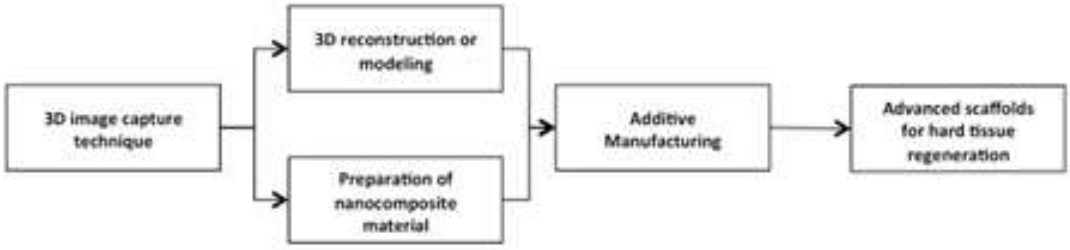

Figure 2.1. Design and production process of customized PCL/HA scaffolds for hard tissue regeneration.

Computed tomography (CT) was performed to acquire the image and, consequently, the shape and size of a human mandible. The obtained point clouds were appropriately processed. Rapidform software and Materialise Magics were used for the reconstruction of the 3D model.

2.3. Results and Discussion

The roles of reverse engineering [2,26-29], computer-aided design, and finite element analysis [30-34] have been frequently stressed in the literature. In addition, over previous years, the advances in methodologies and design strategies have pushed the research towards the development of novel structures for different fields of application [2,35-41]. The functional behavior of 3D additive manufactured scaffolds is clearly dependent on the geometric and architectural features, as well as on the pore spatial distribution. Concerning the development of additive manufactured scaffolds, many studies have already demonstrated the possibility of properly tailoring the road width (RW) by varying the instrument and process parameters at a fixed nozzle size [2,25]. In the current study, a nozzle with an inner diameter of 400 μm was employed to manufacture the PCL/HA nanocomposite

scaffolds. In particular, an already considered approach [25] was used to develop additive manufactured PCL scaffolds.

The manufacturing parameters were selected to obtain a value of the RW that was equivalent to the inner nozzle diameter (400 μm), attempting to reduce the fabrication time and to maintain the highest reproducibility without significant alteration of the structural stability of the devices. The results obtained from the experimental analyses evidenced the influence of the investigated parameters (PT, SRV, DV, and ST) on the flow behavior of the material, which clearly resulted in changes in terms of the RW. Such variations provided the 3D scaffolds with different morphological and mechanical features. The obtained stress–strain curves (Figure 2.2) were similar to those found for the 3D additive manufactured scaffolds [16,25].

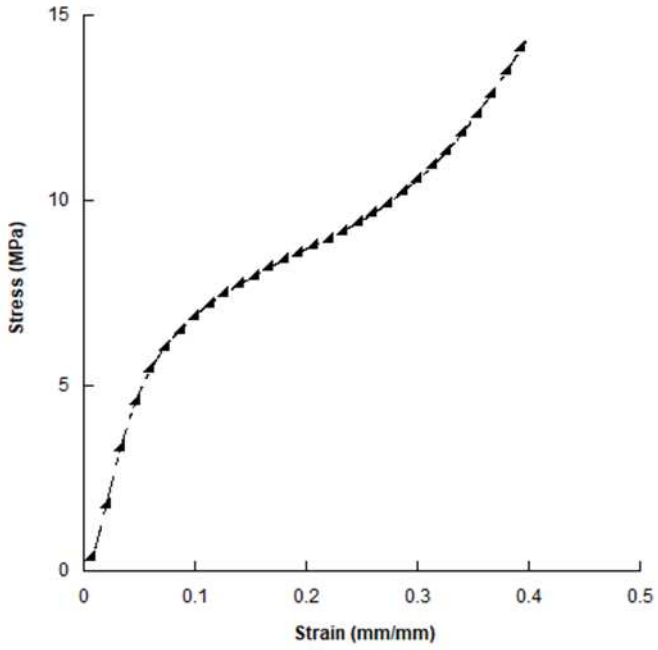

Figure 4.2. Typical results from compression tests. Stress-strain curves for additive manufactured PCL/HA scaffolds with specific lay-down pattern and geometric features, tested up to a strain of 0.4 mm/mm.

The temperature was initially varied (120 °C, 130 °C, and 140 °C) at fixed values of the SRV (30 rpm), DV (10 mm/s), and ST (400 μm).

When the temperature increased from 120 °C to 140 °C, an increase of the RW was evident (Table 2.2).

PT (°C)	RW (µm)	Porosity (%)	Compressive Modulus (MPa)	Maximum Stress (MPa)
120	449 ± 5	60.0 ± 1.2	120.1 ± 11.4	13.5 ± 1.4
130	477 ± 7	55.0 ± 1.2	124.1 ± 12.3	14.8 ± 1.9
140	506 ± 5	50.9 ± 1.2	130.2 ± 14.0	13.3 ± 2.2

Table 2.2. RW, porosity, compressive modulus and maximum stress of 3D PCL/HA scaffolds achieved for different PT values (DV = 10 mm/s, SRV = 30 rpm and ST = 400 µm). Data are reported as mean value ± standard deviation.

Conversely, the porosity values decreased (Table 2.2) due to a reduction in the pore height and the pore width (LG and FG, respectively; data not reported). The findings confirmed the effect of the PT on the morphological features [2]. In particular, a thickening of the filament and a decrease of the scaffold porosity were found with the PT increasing from 120 °C to 140 °C.

In terms of the mechanical properties, the values of the compressive modulus and the maximum stress are shown in Table 2.2.

Although differences in terms of the RW and porosity were observed at different PT values, the results suggested that both the compressive modulus and the maximum stress were not greatly affected if the PT was increased above 120 °C.

The influence of the DV on the morphological and mechanical features was investigated by varying the DV (8, 10, and 12 mm/s) at fixed values of the SRV (30 rpm), ST (400 µm) and PT (120 °C). When the DV increased from 8 to 12 mm/s, the filament thinning provided an increase in the pore width and the scaffold porosity (Table 2.3).

DV (mm/s)	RW (µm)	Porosity (%)	Compressive Modulus (MPa)	Maximum Stress (MPa)
8	479 ± 6	55.6 ± 1.3	128.1 ± 12.0	12.5 ± 1.3
10	449 ± 5	60.0 ± 1.2	120.1 ± 11.4	13.5 ± 1.4
12	431 ± 5	64.2 ± 1.3	91.5 ± 9.2	9.1 ± 0.9

Table 2.3. RW, porosity, compressive modulus and maximum stress of 3D PCL/HA scaffolds achieved for different DV values (PT = 120°C, SRV = 30 rpm and ST = 400 µm). Data are reported as mean value ± standard deviation.

Table 2.3 suggests how the DV may influence both the compressive modulus and the maximum stress of the PCL/HA scaffolds. Specifically, a high value of the DV should negatively affect the mechanical performances of the additive manufactured PCL/HA scaffolds.

Accordingly, in the fast deposition process, the filaments were too stretched, leading to a decrease of the RW and an increase of the porosity [2].

In terms of the compressive modulus and the maximum stress, Table 2.3 shows that the lowest values were obtained for a DV of 12 mm/s. The SRV clearly influences the amount of the extruded/deposited material.

To study the effect of the SRV on the scaffold characteristics, the SRV was varied (20, 25, and 30 rpm) at fixed values of the DV (10 mm/s), ST (400 µm) and PT (120 °C). An increase of the RW was evident with the SRV increasing from 20 to 30 rpm due to the higher amount of extruded material. However, higher SRV values led to a decrease in the pore width (FG), the pore height (LG), and the porosity (Table 2.4).

SRV (rpm)	RW (μm)	Porosity (%)	Compressive Modulus (MPa)	Maximum Stress (MPa)
20	381 ± 6	71.3 ± 1.7	65.6 ± 6.8	9.2 ± 0.8
25	430 ± 5	63.7 ± 1.4	81.3 ± 8.9	9.7 ± 0.8
30	449 ± 5	60.0 ± 1.2	120.1 ± 11.4	13.5 ± 1.4

Table 2.4. RW, porosity, compressive modulus and maximum stress of 3D PCL/HA scaffolds achieved for different SRV values (PT = 120°C, DV = 10 mm/s and ST = 400 μm). Data are reported as mean value ± standard deviation.

As a consequence of the higher SRV values, the thickening of the filament provided the PCL/HA structures with a lower porosity. The results reported in Table 2.4 indicate that the highest values of the compressive modulus and the maximum stress were found for an SRV of 30 rpm. The ST also plays an important role in determining the filament diameter, pore width, pore height, and porosity, thus providing the possibility of tailoring the scaffold characteristics [2,25]. Intuitively, a decrease of the ST values generates a compression of the filaments in the adjacent layers and, hence, a change in the geometry of the filaments, which become more elliptical.

This effect causes an increase of the filament diameter, together with a reduction of the pore width and porosity.

As the ST decreased from 400 to 350 μm, a decrease of the pore height was obviously obtained, as well as an increment of the filament diameter and, consequently, a reduction of the pore width and porosity (Table 2.5).

ST (µm)	RW (µm)	Porosity (%)	Compressive Modulus (MPa)	Maximum Stress (MPa)
350	489 ± 6	46.8 ± 1.3	137.1 ± 13.8	15.2 ± 1.4
380	469 ± 6	53.3 ± 1.2	130.3 ± 13.1	14.4 ± 1.3
400	449 ± 5	60.0 ± 1.2	120.1 ± 11.4	13.5 ± 1.4

Table 2.5. RW, porosity, compressive modulus and maximum stress of 3D PCL/HA scaffolds achieved for different ST values (PT = 120°C, DV=10 mm/s and SRV=30 rpm). Data are reported as mean value ± standard deviation.

For this reason, the ST would influence the mechanical properties. However, Table 2.5 reports the values of the compressive modulus and the maximum stress. The current analysis was focused on the assessment of the optimal set of process/instrument parameters for the fabrication of PCL/HA nanocomposite scaffolds with minimal fabrication time avoiding to compromise the structural integrity and reproducibility features. Accordingly, all the parameters were selected to find a value of the RW that was equivalent to the inner diameter of the employed nozzle (400 µm). As frequently stressed in the literature [2,25], additive manufacturing techniques based on extrusion/injection methods (i.e., fused deposition modeling/3D fiber deposition) enable the possibility of controlling the architectures, pore size, and distribution, consequently leading to the development of 3D scaffolds with tailored mechanical and mass transport properties. In this context, the present study analyzed the effects of the PT, DV, SRV, and ST on the RW, which influence the pore size and porosity, as well as the compressive modulus and the maximum. The interaction of different pairs of parameters on the investigated features of the PCL/HA scaffolds (i.e., RW, compressive modulus, and maximum stress) is reported in Figures 2.3–2.5.

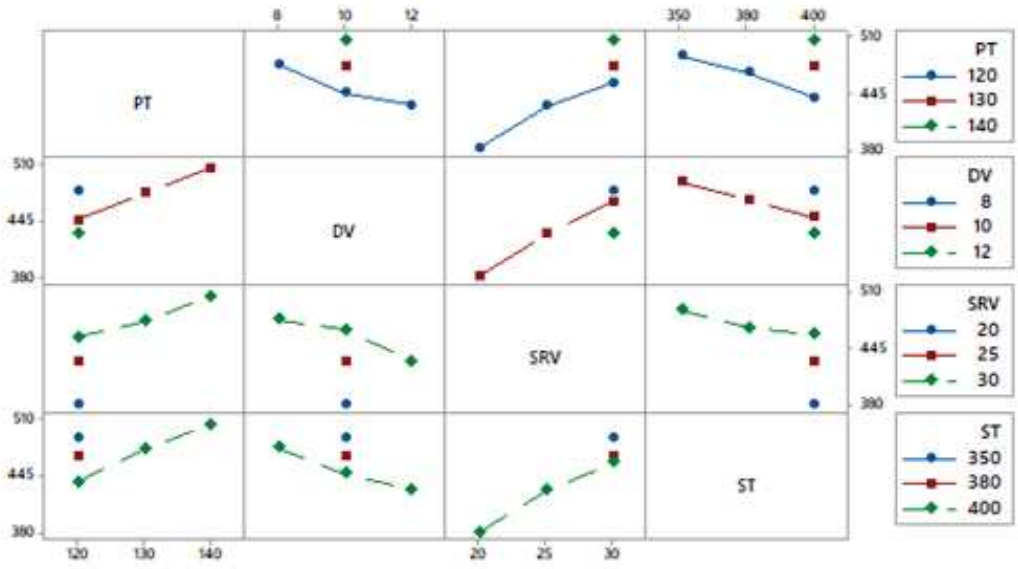

Figure 2.3. Interaction plot for RW (μm).

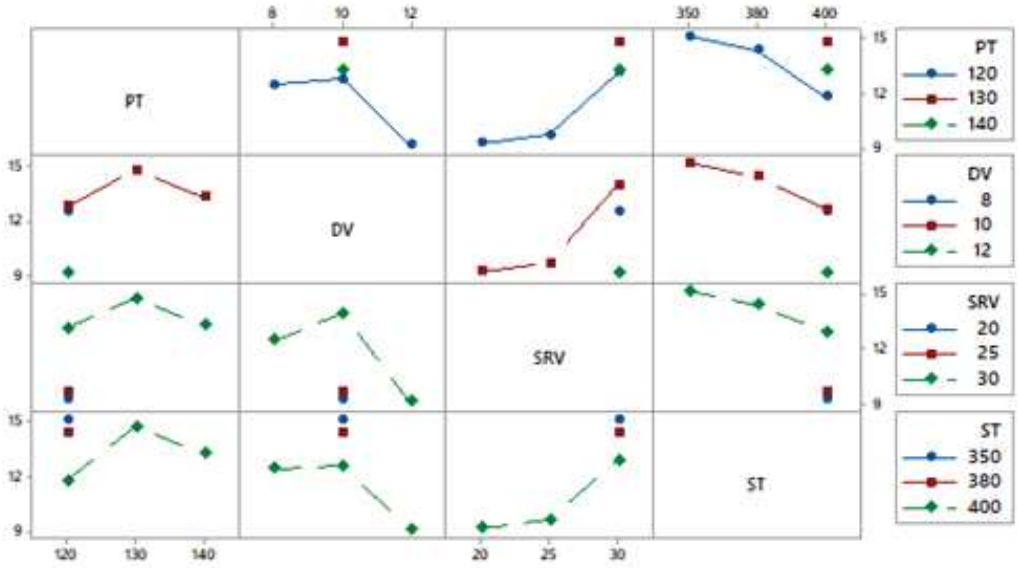

Figure 2.4. Interaction plot for maximum stress (MPa).

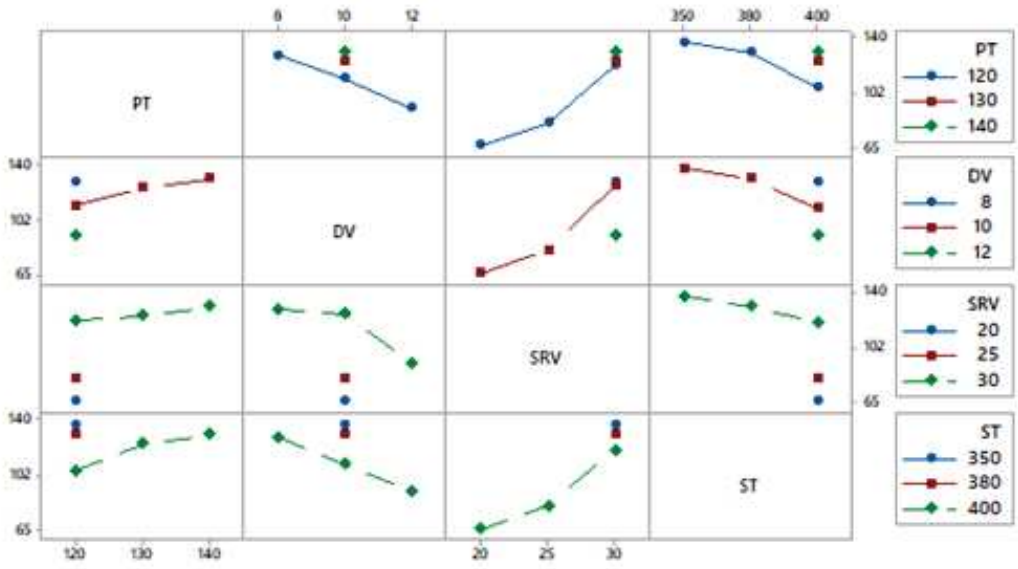

Figure 2.5. Interaction plot for compressive modulus (MPa).

For example, Figure 2.3 illustrates the interaction plot for the RW, reporting the combined effects (PT and DV, PT and SRV, PT and ST) on the RW. Similarly, the interaction plots for the maximum stress and the compressive modulus are shown in Figure 2.4 and 2.5, respectively. Table 2.6 summarises the optimized set of parameters for the manufacturing of 3D PCL/HA (90/10 w/w) scaffolds characterised by a pre-defined value of the RW, pore size, and porosity, without compromising the structural and mechanical characteristics.

PT (°C)	DV (mm/s)	SRV (rpm)	ST (µm)
120	10	30	400

Table 2.6. Optimized set of parameters for the fabrication of PCL/HA (90/10 w/w) scaffolds through a bioextruder system.

The results from the nanoindentation tests on the PCL fibers provided values of hardness ranging from 0.43 ± 0.03 GPa to 0.26 ± 0.02 GPa in the investigated load range (Figure 2.6).

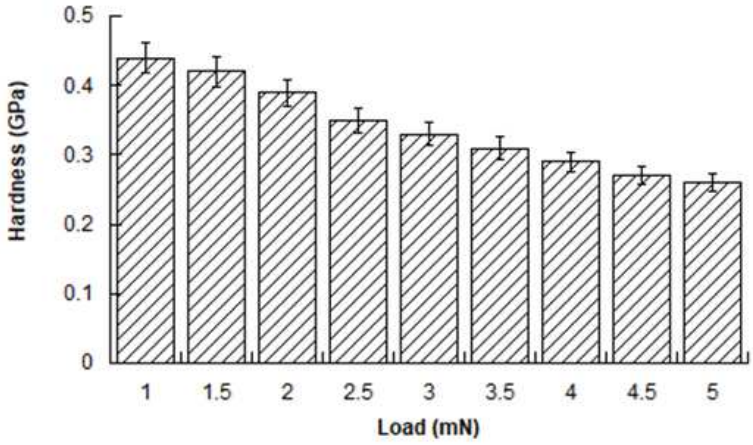

Figure 2.6. Results obtained from nanoindentation tests on PCL fibers. Hardness as a function of the applied load. Data are reported as mean value, error bar represents the standard deviation.

The inclusion of HA nanoparticles led to an increase in the compressive modulus and the fibers hardness. In vitro biological tests were performed to evaluate the influence of the inorganic nanoparticles on the behavior of the hMSCs. Typical results obtained from the Alamar Blue assay are reported in Figure 2.7.

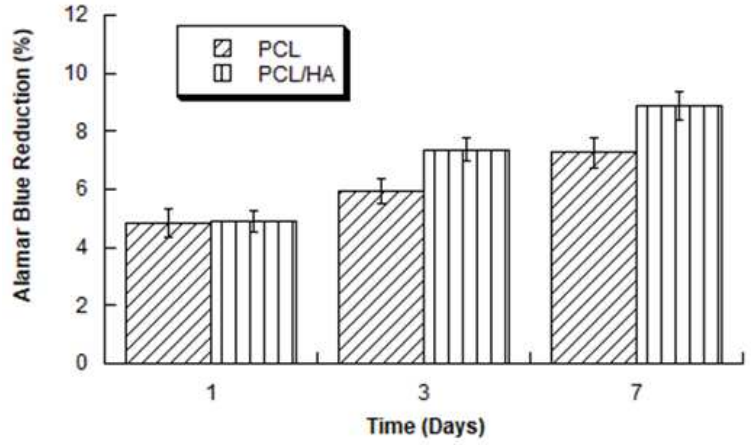

Figure 2.7. Percentage of Alamar Blue Reduction for PCL and PCL/HA scaffolds at 1, 3, and 7 days. Data are reported as mean value, error bar represents the standard deviation.

With regard to the biological performances, the Alamar Blue assay was employed to assess the cell viability and proliferation. This method is based on a redox reaction that occurs in the cell mitochondria.

The percentage of Alamar Blue reduction is related to the number of viable cells. Specifically, a significant increase of Alamar Blue reduction was found over time, indicating that the hMSCs could survive and proliferate throughout the scaffolds. Although no differences were observed between the PCL/HA scaffolds and the PCL structures at day 1, the inclusion of HA significantly enhanced the cell viability/proliferation at day 3 and day 7 (Figure 2.7).

The CLSM images and cell-shape factor further allowed investigation of the cell adhesion and spreading. The shape factor significantly decreased over time for both types of cell-laden constructs, and the typical values are reported in Figure 2.8.

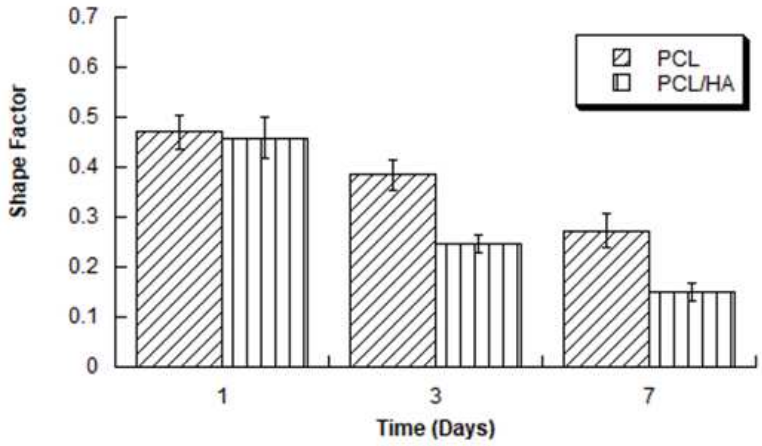

Figure 2.8. Values of shape factor obtained from CLSM images of hMSCs on PCL and PCL/HA nanocomposite scaffolds. Data are reported as mean value and error bar represents the standard deviation.

In comparison to the neat PCL scaffolds, at day 3 and day 7, a lower shape factor was achieved for the PCL/HA nanocomposite structures, even though at day 1 similar values were found for the two types of cell-laden constructs. It is also worth noting that a reduction of the shape factor should

suggest better cell adhesion and spreading, since the lower the shape factor, the more elongated the cell [2,16]. These results confirmed the effect of the HA inclusion in enhancing cell adhesion.

Furthermore, the normalized ALP activity (ALP/DNA) was determined at 7, 14 and 21 days in order to assess early osteogenic differentiation. The ALP/DNA ratio showed a peak value at 14 days for both cell-laden scaffolds (Figure 2.9).

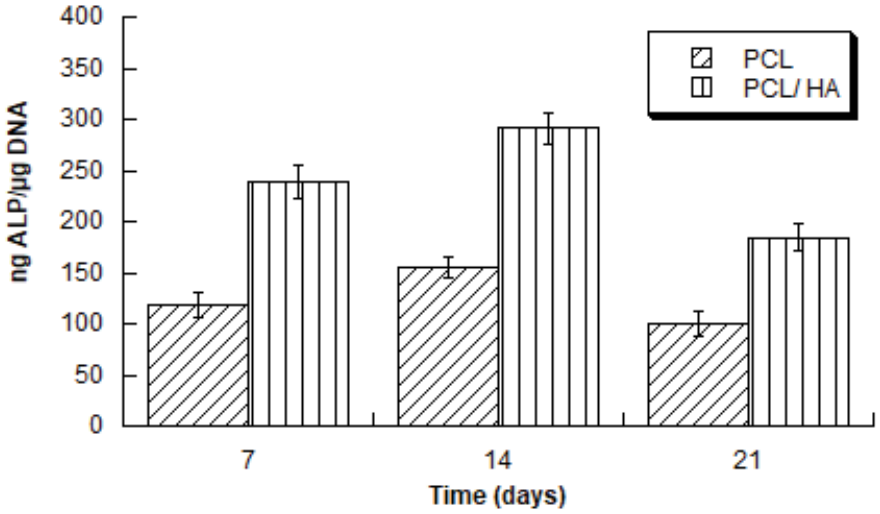

Figure 2.9. Normalized ALP activity (ALP/DNA) measured for PCL and PCL/HA scaffolds at different time points.

At each time point, higher values of normalized ALP activity were found for PCL/HA, if compared to PCL scaffolds. The observed differences were statistically significant. These results clearly demonstrated how the presence of HA led to higher levels of ALP activity and provided an improvement in supporting the osteogenic differentiation of hMSCs.

Finally, considering the obtained results, the reverse engineering approach [2] was also employed to develop customized and functional nanocomposite scaffolds for mandibular defect regeneration (i.e., symphysis and ramus) (Figure 2.10).

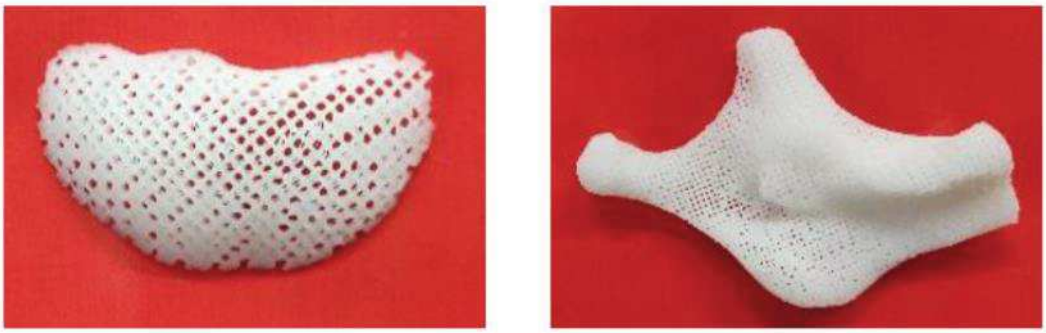

Figure 2.10. Customized PCL/HA scaffolds for mandibular defect regeneration (i.e., symphysis – left, ramus-right).

2.4. Conclusions

A systematic study on the design of PCL/HA scaffolds for hard tissue regeneration was reported in the current research. In particular, 3D PCL/HA scaffolds were designed and analyzed according to a strategy already reported for additive manufacturing of PCL scaffolds, involving techniques based on extrusion/injection methods. The procedure was extended to PCL/HA, considering that the difficulties in processing nanocomposite materials are usually greater than those found for the neat polymers. The neat PCL scaffolds represented the starting point in the design process, and the results from different analyses were briefly summarised. The reported design strategy also aimed to stress the potential of tailoring the performances of 3D additive manufactured scaffolds through an appropriate material–design combination [2]. Similar stress–strain curves were achieved for the polymeric and the nanocomposite scaffolds, even if differences were obtained in terms of the mechanical properties. The inclusion of HA nanoparticles would enhance both the biological and mechanical performances of the PCL scaffolds. Furthermore, the obtained findings demonstrated that the DV and the SRV were the parameters with the highest impact on the investigated features (i.e., the RW, the compressive modulus, and the maximum stress). Benefiting from all the results, as well as from the reverse engineering approach, the feasibility of designing customized scaffolds for mandibular defect regeneration (i.e., ramus and symphysis) was also reported.

2.5. References

[1] J. Lee, M. M. Farag, E. K. Park, J. Lim, H. Yun, A simultaneous process of 3D magnesium phosphate scaffold fabrication and bioactive substance loading for hard tissue regeneration, Material Science and Engineering: C 36(1) (2014), pp. 252-260.

[2] P. Fucile, I. Onofrio, I. Papallo, V. Gallicchio, A. Rega, V. D'Antò, G. Improta, R. De Santis, A. Gloria, T. Russo, Strategies for the design of additively manufactured nanocomposite scaffolds for hard tissue regeneration, ACTA IMEKO, Volume 9, Number 4, (2020), pp. 53 – 59.

[3] A. Oryan, S. Alidati, A. Moshiri, N. Maffulli, Bone regenerative medicine: classic options, novel strategies, and future directions. Journal of Orthopaedic Surgery and Research 9(1) (2014), pp. 18-45.

[4] M. J. Yaszemski, J. B. Oldham, L. Lu, B. L. Currier, Clinical Needs for Bone Tissue Engineering Technology, in: Bone Engineering. J. E. Davies (editor). University of Toronto, Toronto, 2000, ISBN:096869800x; pp. 541-547.

[5] R. Spitzer, C. Perka, K. Lindenhayn, H. Zippel, Matrix engineering for osteogenic differentiation of rabbit periosteal cells using a-tricalcium phosphate particles in a three-dimensional fibrin culture, J Biomed Mater Res A 59(4) (2002), pp. 690-696.

[6] R. Fontanella, D. Accardo, R. Schiano Lo Moriello, L. Angrisani, D. De Simone, An innovative strategy for accurate thermal compensation of gyro bias in inertial units by exploiting a novel Augmented Kalman Filter, Sensors 8(5) (2018) 1457.

[7] G. C. Simon, C. A. Khatri, S. A. Wight, F. W. Wang, Preliminary report on the biocompatibility of a moldable, resorbable, composite bone graft consisting of calcium phosphate cement and poly(lactide-co-glycolide) microspheres, J Orthop Res 20(3) (2002), pp. 473-482.

[8] H. Petite, V. Viateau, W. Bensaid, A. Meunier, C. de Pollak, M. Bourguignon, K. Oudina, L. Sedel, G. Guillemin, Tissueengineered bone regeneration, Nat Biotechnol 18(9) (2000); ISBN:096869800x; pp. 959-963.

[9] D. F. Williams, Perspectives on the contributions of biomaterials and tissue engineering to bone repair, reconstruction and regeneration, in: Bone engineering. J. E. Davies (editor). University of Toronto, Toronto, 2000, ISBN, pp. 577-584.

[10] I. Seto, I. Asahina, M. Oda, S. Enomoto, Reconstruction of the primate mandible with a combination graft of recombinant human bone morphogenetic protein-2 and bone marrow, J Oral Maxillofac Surg 59(1) (2001), pp. 53-61.

[11] C. G. Finkemeier, Bone-grafting and bone-graft substitutes, J Bone Joint Surg 84(3) (2002), pp. 454-464.

[12] L. Angrisani, F. Bonavolontà, A. Liccardo, R. Schiano Lo Moriello, L. Ferrigno, M. Laracca, G. Miele, Multichannel simultaneous data acquisition through a compressive sampling-based approach, Measurement 52 (2014), pp. 156-172.

[13] F. Bonavolontà, A. Tedesco, , R. Schiano Lo Moriello, A. Tufano, Enabling wireless technologies for industry 4.0: State of the art., Proc. of IEEE International Workshop on Measurement and

Networking, M & N 2017, Naples, Italy, 27-29 September 2017, pp. 1-5.

[14] S. N. Khan, E. Tomin, J. M. Lane, Clinical applications of bone graft substitutes, Orthop Clin North Am 31(3) (2000), pp. 389-398.

[15] F. P. W. Melchels, M. A. N. Domingos, T. J. Klein, J. Malda, P. J. Bartolo, D. W. Hutmacher, Additive manufacturing of tissues and organs, Prog Polym Sci 37(8) (2012), pp. 1079-1104.

[16] M. Domingos, A. Gloria, J. Coelho, P. Bartolo, J. Ciurana, Threedimensional printed bone scaffolds: The role of nano/microhydroxyapatite particles on the adhesion and differentiation of human mesenchymal stem cells, Proc. Inst. Mech. Eng. H. 231(6)(2017), pp. 555-564.

[17] S. H. Lee, H. Shin, Matrices and scaffolds for delivery of bioactive molecules in bone and cartilage tissue engineering, Adv Drug Deliv Rev 59 (2007), pp. 339-359.

[18] E. J. Anderson, M. L. K. Tate, Design of tissue engineering scaffolds as delivery devices for mechanical and mechanically modulated signals, Tissue Eng 13(10) (2007), pp. 2525-2538.

[19] M. A. Woodruff, D. W. Hutmacher, The return of a forgotten polymer – polycaprolactone in the 21st century, Prog Polym Sci 35(10) (2010), pp. 1217-1256.

[20] J. Rich, T. Jaakkola, T. Tirri, T. Närhi, A. Yli-Urpo, J. Seppälä, In vitro evaluation of poly(ε-caprolactone-co-DL-lactide)/bioactive glass composites, Biomaterials 23(10) (2002), pp. 2143-2150.

[21] H. W. Kim, J. C. Knowles, H. E. Kim, Hydroxyapatite/poly(εcaprolactone) composite coatings on hydroxyapatite porous bone scaffold for drug delivery, Biomaterials 25 (2004), pp. 1279-1287.

[22] S. M. S. Bidic, J. W. Calvert, K. Marra, P. Kumta, P. Campbell, R. Mitchell, W. Wigginton, J. O. Hollinger, L. Weiss, M. P. Mooney, Rabbit calvarial wound healing by means of seeded caprotite® scaffolds, J Dent Res 82(2) (2003), pp. 131-135

[23] M. Fini, G. Giavaresi, N. N. Aldini, P. Torricelli, R. Botter, D. Beruto, R. Giardino, A bone substitute composed of polymethylmethacrylate and α-tricalcium phosphate: results in terms of osteoblast function and bone tissue formation, Biomaterials 23(23) (2002), pp. 4523-4531.

[24] S. J. Peter, L. Lu, D. J. Kim, A. G. Mikos, Marrow stromal osteoblast function on a poly(propylene fumarate)/β-tricalcium phosphate biodegradable orthopaedic composite, Biomaterials 21(12) (2000), pp. 1207-1213.

[25] M. Domingos, F. Chiellini, A. Gloria, L. Ambrosio, P. Bartolo, E. Chiellini, Effect of process parameters on the morphological and mechanical properties of 3D bioextruded poly(εcaprolactone) scaffolds, Rapid Prototyping Journal 18 (2012), pp. 56-67

[26] M. Martorelli, P. Ausiello, R. Morrone, A new method to assess the accuracy of a Cone Beam Computed Tomography scanner by using a non-contact reverse engineering technique, Journal of Dentistry 42(4) (2014), pp. 460-465.

[27] M. Calì, D. Speranza, M. Martorelli, Dynamic Spinnaker Performance through digital photogrammetry, numerical analysis and experimental tests, Advances on Mechanics, Design Engineering and Manufacturing. Springer, Cham (2017), pp. 585- 595.

[28] V. Pagliarulo, F. Farroni, P. Ferraro, A. Lanzotti, M. Martorelli, P. Memmolo, D. Speranza, F. Timpone, Combining ESPI with laser scanning for 3D characterization of racing tyres sections, Optics and Lasers in Engineering 104 (2018), pp. 71-77.

[29] M. Martorelli, C. Pensa, D. Speranza, Digital photogrammetry for documentation of maritime heritage, Journal of Maritime Archaeology 9(1) (2014), pp. 81-93.

[30] P. Ausiello, S. Ciaramella, M. Martorelli, A. Lanzotti, A. Gloria, D. C. Watts, CAD-FE modeling and analysis of class II restorations incorporating resin-composite, glass ionomer and glass ceramic materials, Dental Materials 33(12) (2017), pp. 1456- 1465.

[31] P. Ausiello, S. Ciaramella, M. Martorelli, A. Lanzotti, F. Zarone, D. C. Watts, A. Gloria, Mechanical behavior of endodontically restored canine teeth: Effects of ferrule, post material and shape, Dental Materials 33(12) (2017), pp. 1466–1472.

[32] F. Caputo, A. De Luca, A. Greco, S. Maietta, M. Bellucci, FE simulation of a SHM system for a large radio-telescope, International Review on Modelling and Simulations 11(1) (2018), pp. 5-14.

[33] L. Angrisani, F. Bonavolonta, R. Schiano Lo Moriello, A. Andreone, R. Casini, G. Papari, D. Accardo, First steps towards an innovative compressive sampling based-THz imaging system for early crack detection on aereospace plates, Proc. of IEEE Metrology for Aerospace (MetroAeroSpace), Benevento, Italy, 29-30 May 2014, pp. 488-493.

[34] A. Gloria, S. Maietta, M. Martorelli, A. Lanzotti, D. C. Watts, P. Ausiello, FE analysis of conceptual hybrid composite endodontic post designs in anterior teeth, Dental Materials 34(7) (2018), pp. 1063-1071.

[35] L. Angrisani, F. Bonavolontà, A. Liccardo, R. Schiano Lo Moriello, On the use of LORA technology for logic selectivity in MV distribution networks, Energies, 11(11) (2018), 3079, 34 pages.

[36] L. Angrisani, F. Bonavolontà, A. Liccardo, R. Schiano Lo Moriello, F. Serino, Smart power meters in augmented reality environment for electricity consumption awareness, Energies, 11 (9) (2018), 2303, 17 pages.

[37] F. Bonavolontà, M. D'Arco, G. Ianniello, A. Liccardo, R. Schiano Lo Moriello, L. Ferrigno, M. Laracca, G. Miele, On the suitability of compressive sampling for the measurement of electrical power quality, Proc. of Instrumentation and Measurement Technology Conference (I2MTC), Minneapolis, USA, 6-9 May 2013, pp. 126- 131.

[38] A. Baccigalupi, A. Liccardo, The Huang Hilbert Transform for evaluating the instantaneous frequency evolution of transient signals in non-linear systems, Measurement 86 (2016), pp. 1-13.

[39] C. Landi, A. Liccardo, N. Polese, Remote laboratory activities to support experimental session for undergraduate measurements courses, Proc. of IEEE Instrumentation and Measurement Technology Conference (IMTC), Sorrento, Italy, 24-27 April 2006, pp. 851-856.

[40] P. Bifulco, G. D. Gargiulo, G. D'Angelo, A. Liccardo, M. F. Romano, F. Clemente, M. Cesarelli, Monitoring of respiration, seismocardiogram and heart sounds by a PVDF piezo film sensor, Proc. of XX IMEKO TC4 International Symposium, Benevento, Italy, 15-17 Sept. 2014, pp.786-789. Online [accessed 05 December 2020] https://www.imeko.org/publications/tc4-2014/IMEKO-TC4- 2014-285.pdf.

[41] M. Giordano, P. Ausiello, M. Martorelli, R. Sorrentino, Reliability of computer designed surgical guides in six implant rehabilitations with two years follow-up, Dental Materials 28(9) (2012), pp. e168- e177.

Chapter 3

An engineered design of 3D additive manufactured nanocomposite scaffolds with optimized properties

3.1. Introduction

A great interest has been devoted craniofacial tissue engineering over the past two decades [1-3]. Specifically, a significant contribution was clearly due to the research and development in the field of bone augmentation leading to tissue engineering as an alternative treatment option in dentistry and medicine [1-3].

In this scenario, biomaterials play a crucial for tissue regeneration as it is widely recognized how their properties may be properly modulated by varying the composition and, in many cases, the architecture, in order to regulate the cell microenvironment during the tissue formation process, also controlling the rate of regeneration [3,4].

In general, biomaterials are employed to develop scaffolds which should allow cell migration, proliferation and differentiation, thus promoting new tissue formation [1,2,5-13].

With regard to craniofacial bone regeneration and augmentation, a wide range of organic and inorganic biomaterials have been investigated [14-18]. As an example, bioceramics such as calcium phosphate (CaP) have been considered to fabricate “inorganic” scaffolds, whereas synthetic and natural biopolymers have been taken into account to develop “organic” scaffolds [10,19-29].

The great effort to mimic the organic-inorganic composition and the structure of the natural bone, where nanocrystallites of hydroxyapatite reinforce the fibrils of a natural organic polymer (collagen), has driven the research towards the design of strong and durable biomaterials [3,10-13,28,29].

In the current chapter, an engineered design of 3D additive manufactured scaffolds with tailored properties was reported as a potential strategy to develop advanced devices for craniofacial bone regeneration and augmentation.

3.2. Materials and Methods

Design and fabrication of 3D nanocomposite PCL/HA scaffolds

Poly(ε-caprolactone)/hydroxyapatite (PCL/HA) nanocomposite pellets were initially prepared and then processed to build 3D porous scaffolds using an additive manufacturing technique (based on extrusion/injection methods (3D fiber deposition). As described in Chapter 2, PCL (Mw = 65,000; Sigma-Aldrich, St. Louis, MO) pellets were dissolved in tetrahydrofuran (THF; Sigma-Aldrich, St. Louis, MO) while stirring at room temperature. HA nanoparticles and ethanol were then added to the solution. A polymer/filler weight ratio (w/w) of 90/10 was employed. An ultrasonic bath (Branson 1510 MT, Danbury, CT) was used for the dispersion of the HA nanoparticles in the PCL/THF solution.

The obtained PCL/HA nanocomposite pellets were used for the fabrication of 3D fiber-deposited nanocomposite scaffolds. In particular, 3D block-shaped scaffolds (5.0 mm in length – L_0, 5.0 mm in width – W_0 and 8.0 mm in height – H_0) were built layer-by-layer, depositing the fibers along specific directions according to specific lay-down patterns. The material was extruded through a needle and the fiber was deposited at a speed of 30 mm/min The second deposition angle was varied generating three different lay-down patterns (0°/45°, 0°/60°, 0°/90°).

Mechanical Analysis

Compression tests were carried out on 3D additive manufactured scaffolds (length—L_0 of 5.0 mm, width—W_0 of 5.0 mm, height—H_0 of 8.0 mm). The specimens were tested to a strain of 40% at a rate of 1 mm/min, using an INSTRON 5566 testing machine. The “apparent” stress (σ) and strain (ε) were

calculated (Equations 3.1 and 3.2) considering the measured force (F), the initial cross-sectional area ($A_0=L_0 \cdot W_0$) and the height variation (ΔH) of the specimen.

$$\sigma = \frac{F}{L_0 \cdot W_0} \quad (3.1)$$

$$\varepsilon = \frac{\Delta H}{H_0} \quad (3.2)$$

Biological Analysis

An already reported procedure was used for cell culture and cell viability/proliferation assessment [30,31]. In brief, human mesenchymal stem cells (hMSCs, Millipore, Germany), at the fourth passage, were cultured in DMEM (Microtech, Italy) supplemented with 10% (v/v) FBS (Gibco™, Thermo Fisher Scientific), 2 mM L-glutamine and antibiotics (penicillin G sodium 100 U/mL, streptomycin 100 g/mL) at 37 °C and 5% CO_2. 3D additive manufactured PCL and PCL/HA scaffolds were prepared by soaking the structures in a solution of ethanol and antibiotics (penicillin/streptomycin), washed in PBS (Sigma-Aldrich, Milan, Italy) and pre-wetted in FBS. hMSCs were seeded onto the scaffolds and a density of 1.0×10^4 cells/sample was employed. The cell-laden scaffolds were incubated for 2 h (37 °C, 5% CO_2) and culture medium was then added to each well in a multi-well plate.

The Alamar Blue assay (AbD Serotec Ltd., Kidlington, UK) was employed to analyse cell viability and proliferation. At 1, 3 and 7 days after cell seeding, the different kinds of cell-laden scaffolds were rinsed with PBS (Sigma–Aldrich, Milan, Italy), and DMEM without Phenol Red (HyClone, Cramlington, UK) containing 10% (v/v) Alamar Blue was added for each sample. The cell-laden scaffolds were incubated for 4 h (37 °C, 5% CO_2). The optical density was measured at specific wavelengths (570 and 595 nm) through a spectrophotometer (Sunrise, Tecan, Männedorf, Zurich,

Switzerland). The percentage of Alamar Blue reduction was evaluated at different time points. The experiments were done at least three times in triplicate.

Design of Experiments

The experiments were designed to study the effects of two variable factors on five measured responses. The variable factors were the amount of HA and the second deposition angle. The measured responses were two mechanical (i.e., compressive modulus and maximum stress) and three biological ones (i.e., Alamar Blue reduction at 1, 3 and 7 days). The response surface methodology was employed to visualize the regions with several properties, whereas the composite desirability was used to find the optimized solution.

Statistical Analysis

The significance of the effects of the factors was evaluated by ANOVA. The significance level was set to 0.05.

3.3. Results and Discussion

Mechanical and biological properties of the different kinds of additive manufactured PCL/HA nanocomposite scaffolds analyzed in the current research are reported in Table 3.1, according to the amount of HA and second deposition angle.

HA (wt %)	2nd dep. angle (°)	Maximum Stress (MPa)	Modulus (MPa)	Alamar Blue red. - day 1 (%)	Alamar Blue red.– day 3 (%)	Alamar Blue red. - day 7 (%)
0	45	4.4 ± 0.5	31.8 ± 4.0	4.3 ± 0.2	6.0 ± 0.1	6.7 ± 0.2
0	60	6.5 ± 0.7	43.0 ± 4.4	4.3 ± 0.2	6.1 ± 0.1	6.9 ± 0.2
0	90	8.7 ± 0.8	61.7 ± 6.1	4.4 ± 0.2	7.0 ± 0.1	7.8 ± 0.2
5	45	6.2 ± 0.7	44.5 ± 5.6	4.4 ± 0.2	7.2 ± 0.2	8.5 ± 0.3
5	60	7.9 ± 0.7	56.8 ± 5.8	4.5 ± 0.2	7.4 ± 0.2	8.5 ± 0.2
5	90	11.3 ± 0.9	85.1 ± 8.5	4.6 ± 0.2	9.3 ± 0.2	10.5 ± 0.3
10	45	8.8 ± 0.5	89.4 ± 8.0	4.5 ± 0.2	7.7 ± 0.2	8.5 ± 0.2
10	60	12.7 ± 1.2	100.2 ± 9.4	4.6 ± 0.2	7.8 ± 0.3	9.0 ± 0.3
10	90	16.5 ± 1.4	118.2 ± 9.8	4.6 ± 0.2	9.8 ± 0.3	11.0 ± 0.4

Table 3.1. Results from experimental tests performed on 3D additive manufactured PCL/HA scaffolds with different amount of HA and second deposition angle: mechanical (i.e., maximum stress and modulus) and biological responses (i.e., Alamar Blue reduction at 1, 3 and 7 days) reported as mean ± standard deviation.

The main effects plots (left) and interaction plots (right) of the two variable factors, amount of HA (wt%) and second deposition angle are reported in Figures 3.1 and 3.2. HA was selected to improve the mechanical and biological performance of the additive manufactured scaffolds. Its positive effects on compressive maximum stress and modulus as well as on the Alamar Blue reduction at 1, 3 and 7 days were observed.

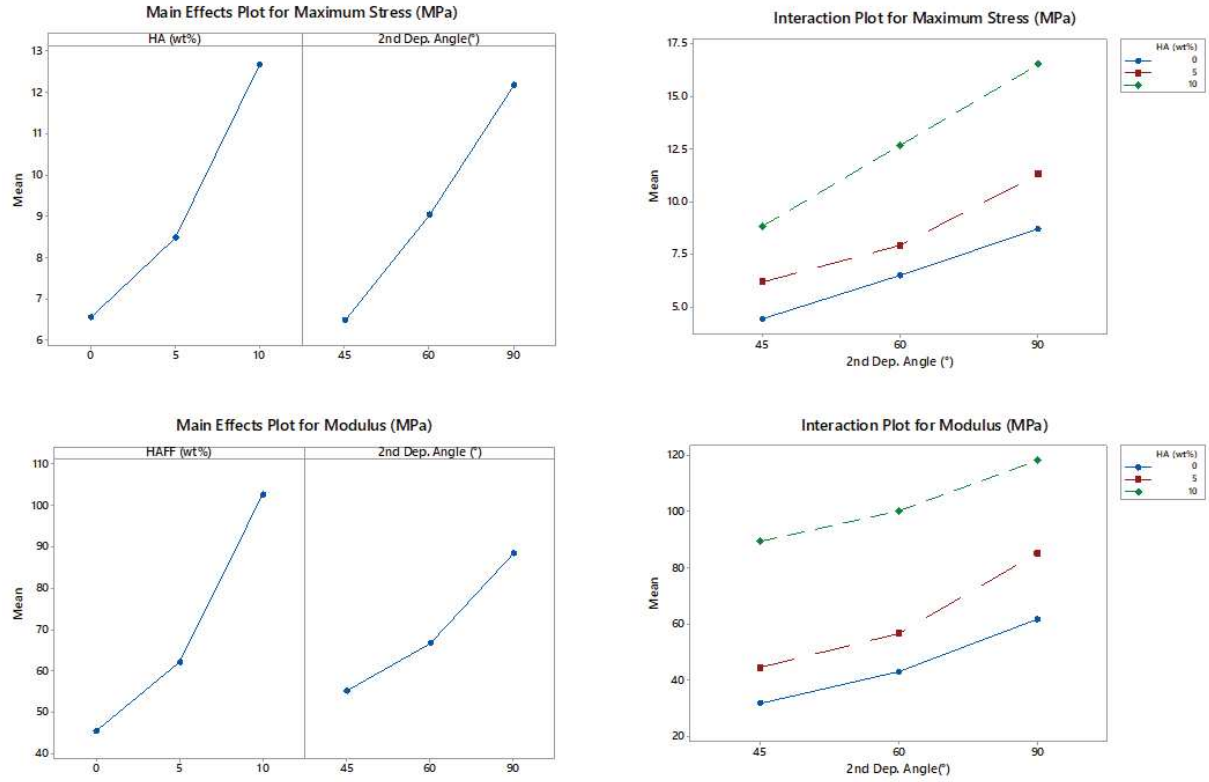

Figure 3.1. The main effects plots (left) and interaction plots (right) of the variable factors for the mechanical responses (maximum stress and modulus).

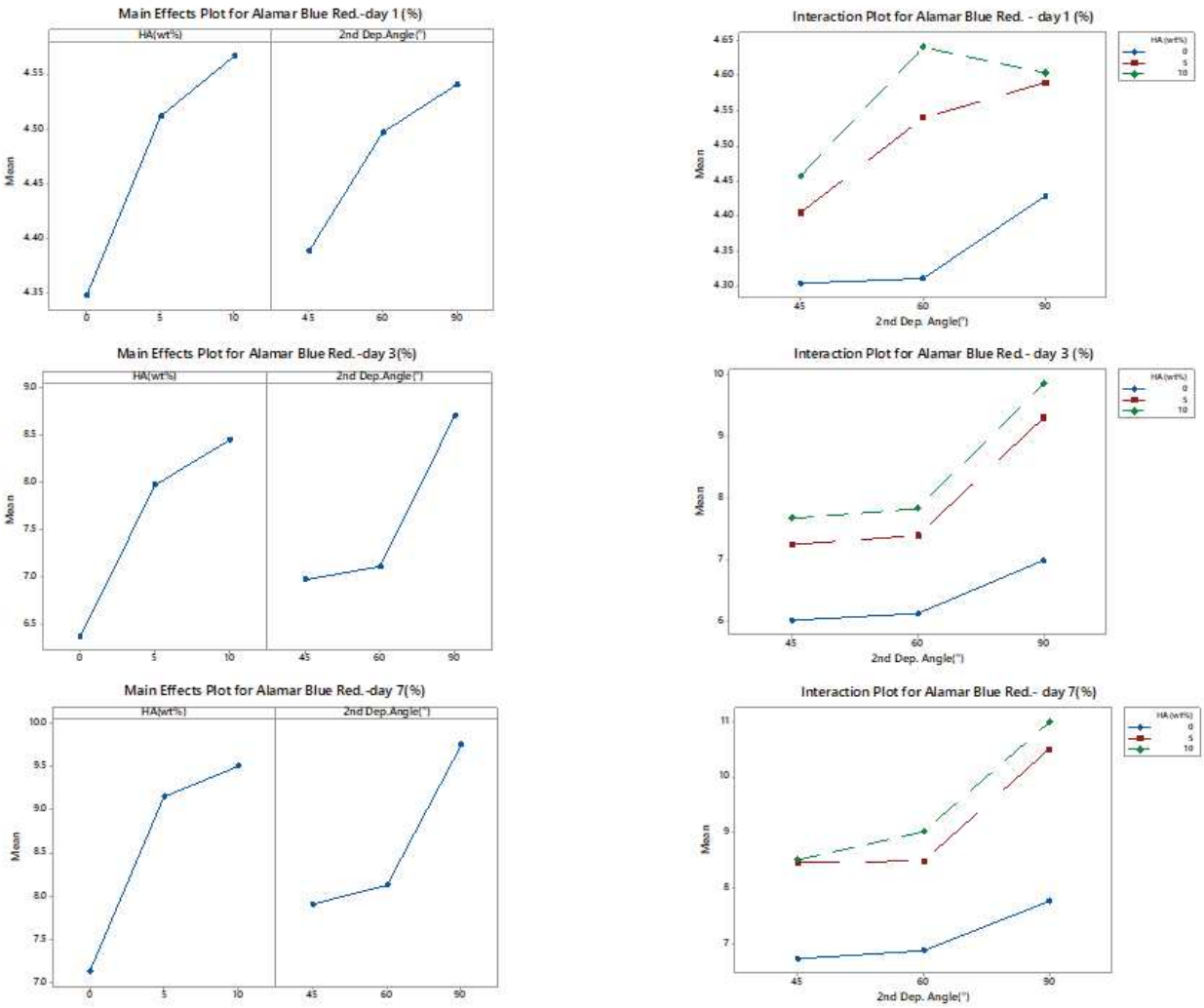

Figure 3.2. The main effects plots (left) and interaction plots (right) of the variable factors for biological responses (Alamar Blue reduction at 1, 3 and 7 days).

In the current research the analysis of variance (ANOVA) was selected as a useful tool for the assessment of the significance of each factor as well as of the interactions between the factors with respect to a specific response. As frequently reported, the factors may be investigated in two or more levels and the predictive capability of the developed regression model is clearly related to the number of levels selected for the factors.

Many studies have frequently reported how a linear model can be employed to match the requirements by varying the factors in two levels (i.e., high and low levels). Anyway, for deeper investigations, more than two levels may be selected for the factors, thus leading to the development of a higher

order regression model. In such case, the factor interactions of higher degree may be assessed and the curvature in the response plot may be also taken into account.

Accordingly, in the current study, ANOVA was implemented as two factors (i.e., amount of HA and second deposition angle) were analyzed. The amount of HA and the second deposition angle were varied in three levels and regression models were developed, also involving the interaction of such two factors.

Considering the full model, the ANOVA tables related the full responses are reported in Tables 3.2-3.6.

Source	DF	Seq SS	Contribution	Adj SS	Adj MS	F-Value	P-Value
Model	5	553.848	94.63%	553.848	110.770	137.45	0.000
Linear	2	522.761	89.32%	537.865	268.932	333.71	0.000
HA (wt %)	1	282.465	48.26%	294.305	294.305	365.19	0.000
2nd dep. Angle (°)	1	240.296	41.06%	243.560	243.560	302.22	0.000
Square	2	17.025	2.91%	17.025	8.513	10.56	0.000
HA*HA	1	12.891	2.20%	12.891	12.891	16.00	0.000
2nd dep. angle*2nd dep. angle	1	4.134	0.71%	4.134	4.134	5.13	0.029
2-Way Interaction	1	14.062	2.40%	14.062	14.062	17.45	0.000
HA * 2nd dep. angle	1	14.062	2.40%	14.062	14.062	17.45	0.000
Error	39	31.430	5.37%	31.430	0.806		
Lack-of-Fit	3	3.350	0.57%	3.350	1.117	1.43	0.250
Pure Error	36	28.080	4.80%	28.080	0.780		
Total	44	585.278	100.00%				

Table 3.2. Analysis of variance for maximum stress.

Source	DF	Seq SS	Contribution	Adj SS	Adj MS	F-Value	P-Value
Model	5	34357.6	94.25%	34357.6	6871.5	127.94	0.000
Linear	2	32936.7	90.36%	32194.5	16097.2	299.72	0.000
HA (wt%)	1	24447.3	67.07%	23966.1	23966.1	446.23	0.000
2nd dep. Angle (°)	1	8489.5	23.29%	8228.3	8228.3	153.20	0.000
Square	2	1419.2	3.89%	1419.2	709.6	13.21	0.000
HA*HA	1	1417.7	3.89%	1417.7	1417.7	26.40	0.000
2nd dep. angle*2nd dep. angle	1	1.5	0.00%	1.5	1.5	0.03	0.868
2-Way Interaction	1	1.6	0.00%	1.6	1.6	0.03	0.863
HA * 2nd dep. angle	1	1.6	0.00%	1.6	1.6	0.03	0.863
Error	39	2094.6	5.75%	2094.6	53.7		
Lack-of-Fit	3	255.6	0.70%	255.6	85.2	1.67	0.191
Pure Error	36	1839.0	5.05%	1839.0	51.1		
Total	44	36452.2	100.00%				

Table 3.3. Analysis of variance for compressive modulus.

Source	DF	Seq SS	Contribution	Adj SS	Adj MS	F-Value	P-Value
Model	5	0.57445	28.03%	0.57445	0.114891	3.04	0.021
Linear	2	0.51242	25.00%	0.52542	0.262710	6.94	0.003
HA (wt%)	1	0.36085	17.60%	0.35206	0.352062	9.31	0.004
2nd dep. angle	1	0.15158	7.39%	0.17336	0.173358	4.58	0.039
Square	2	0.06179	3.01%	0.06179	0.030895	0.82	0.449
HA*HA	1	0.02933	1.43%	0.02933	0.029326	0.78	0.384
2nd dep. angle*2nd dep. angle	1	0.03246	1.58%	0.03246	0.032464	0.86	0.360
2-Way Interaction	1	0.00024	0.01%	0.00024	0.000243	0.01	0.937
HA (wt%)*2nd dep. angle	1	0.00024	0.01%	0.00024	0.000243	0.01	0.937
Error	39	1.47534	71.97%	1.47534	0.037829		
Lack-of-Fit	3	0.05065	2.47%	0.05065	0.016884	0.43	0.735
Pure Error	36	1.42468	69.50%	1.42468	0.039575		
Total	44	2.04979	100.00%				

Table 3.4. Analysis of variance for Alamar Blue reduction at day 1.

Source	DF	Seq SS	Contribution	Adj SS	Adj MS	F-Value	P-Value
Model	5	65.8651	96.46%	65.8651	13.1730	212.60	0.000
Linear	2	58.6594	85.91%	56.8599	28.4300	458.84	0.000
HA (wt%)	1	32.5648	47.69%	34.2282	34.2282	552.42	0.000
2nd dep. angle	1	26.0946	38.22%	22.6317	22.6317	365.26	0.000
Square	2	5.0558	7.40%	5.0558	2.5279	40.80	0.000
HA*HA	1	3.1781	4.65%	3.1781	3.1781	51.29	0.000
2nd dep. angle*2nd dep. angle	1	1.8777	2.75%	1.8777	1.8777	30.31	0.000
2-Way Interaction	1	2.1499	3.15%	2.1499	2.1499	34.70	0.000
HA*2nd dep. angle	1	2.1499	3.15%	2.1499	2.1499	34.70	0.000
Error	39	2.4164	3.54%	2.4164	0.0620		
Lack-of-Fit	3	0.7061	1.03%	0.7061	0.2354	4.95	0.006
Pure Error	36	1.7103	2.50%	1.7103	0.0475		
Total	44	68.2816	100.00%				

Table 3.5. Analysis of variance for Alamar Blue reduction at day 3.

Source	DF	Seq SS	Contribution	Adj SS	Adj MS	F-Value	P-Value
Model	5	82.9706	96.41%	82.9706	16.5941	209.59	0.000
Linear	2	71.7269	83.35%	70.4542	35.2271	444.92	0.000
HA (wt%)	1	42.6684	49.58%	44.8180	44.8180	566.06	0.000
2nd dep. angle	1	29.0586	33.77%	25.6362	25.6362	323.79	0.000
Square	2	8.4830	9.86%	8.4830	4.2415	53.57	0.000
HA (wt%)*HA (wt%)	1	6.9987	8.13%	6.9987	6.9987	88.39	0.000
2nd dep. angle*2nd dep. angle	1	1.4843	1.72%	1.4843	1.4843	18.75	0.000
2-Way Interaction	1	2.7606	3.21%	2.7606	2.7606	34.87	0.000
HA (wt%)*2nd dep. angle	1	2.7606	3.21%	2.7606	2.7606	34.87	0.000
Error	39	3.0878	3.59%	3.0878	0.0792		
Lack-of-Fit	3	0.5863	0.68%	0.5863	0.1954	2.81	0.053
Pure Error	36	2.5015	2.91%	2.5015	0.0695		
Total	44	86.0584	100.00%				

Table 3.6. Analysis of variance for Alamar Blue reduction at day 7.

Table 3.2-3.6 list the p-values for individual factor effect of both first and second order as well as the two-way interaction. The p-value provided information on the significance of a specific analyzed term. Statistically significant effects were considered in the least square regression model when p-values were lower than 0.05 ($p<0.05$).

Based on the obtained findings, in Tables 3.3 and 3.4 some sources were not statistically significant. Accordingly, the above reported effects were suitably eliminated in order to generate the regression model for the responses. The Pareto chart was also used for the determination of the magnitude and the importance of the effects, showing the absolute values of the standardized effects from the largest effect to the smallest one (Figures 3.3 and 3.4).

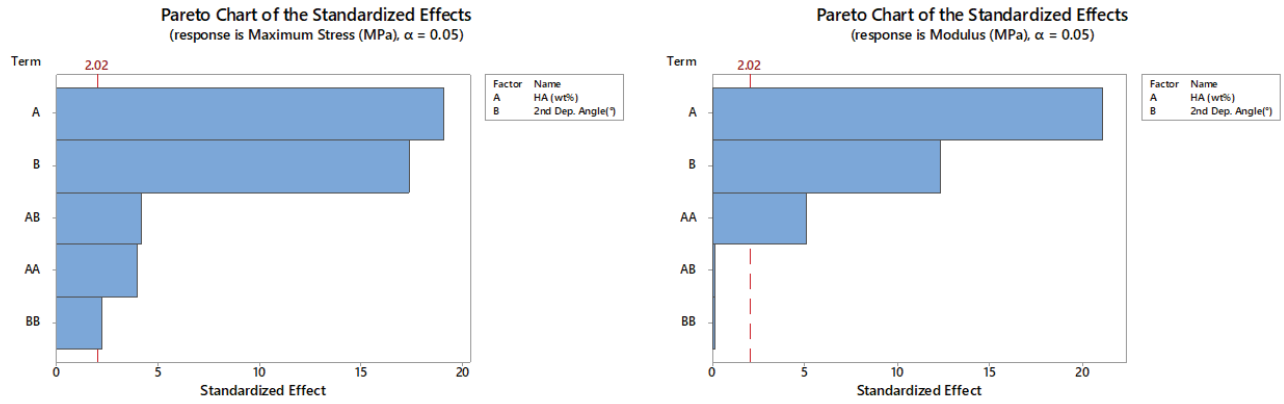

Figure 3.3. Pareto chart of the standardized effects (maximum stress and modulus).

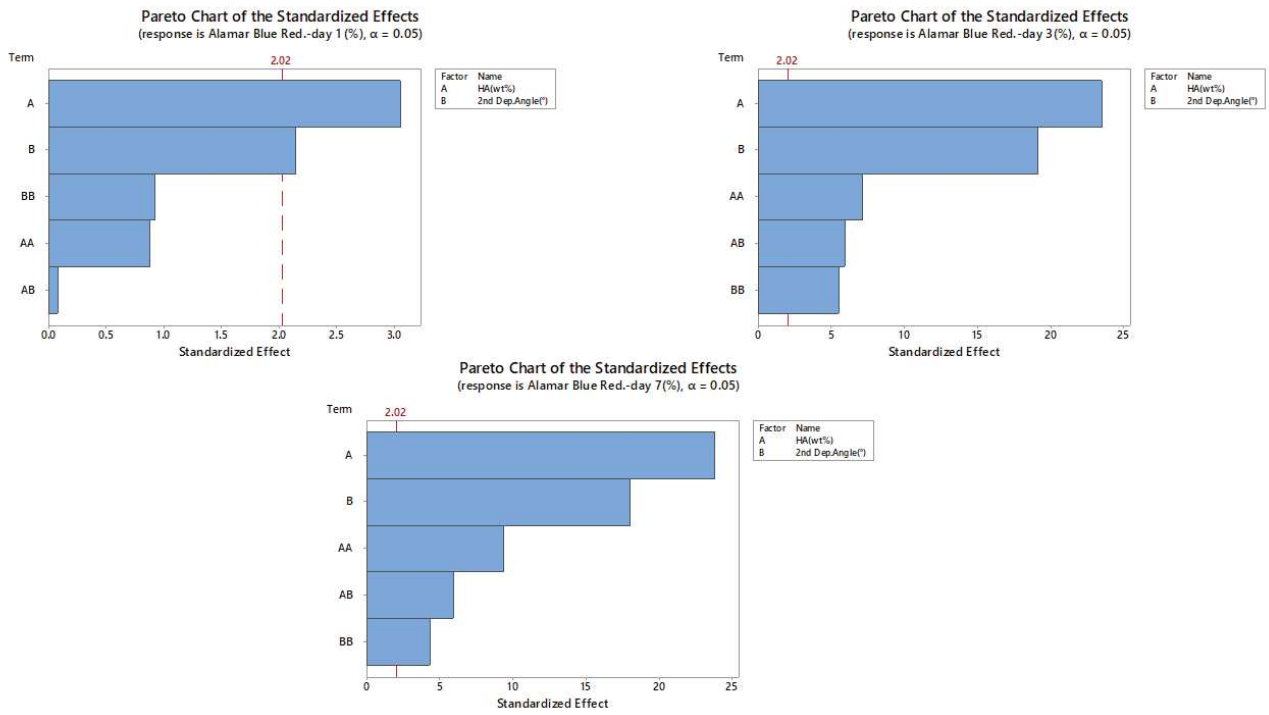

Figure 3.4. Pareto chart of the standardized effects (Alamar Blue reduction at 1, 3 and 7 days).

On the Pareto chart, the bars crossing the reference line result statistically significant.

Tables 3.7 and 3.8 reports the ANOVA results for the reduced model of the compressive modulus and Alamar Blue reduction at day 1.

Source	DF	Seq SS	Contribution	Adj SS	Adj MS	F-Value	P-Value
Model	3	34354.5	94.25%	34354.5	11451.5	223.82	0.000
Linear	2	32936.7	90.36%	32936.7	16468.4	321.87	0.000
HA (wt%)	1	24447.3	67.07%	24447.3	24447.3	477.81	0.000
2nd dep. angle	1	8489.5	23.29%	8489.5	8489.5	165.92	0.000
Square	1	1417.7	3.89%	1417.7	1417.7	27.71	0.000
HA (wt%)*HA (wt%)	1	1417.7	3.89%	1417.7	1417.7	27.71	0.000
Error	41	2097.8	5.75%	2097.8	51.2		
Lack-of-Fit	5	258.7	0.71%	258.7	51.7	1.01	0.424
Pure Error	36	1839.0	5.05%	1839.0	51.1		
Total	44	36452.2	100.00%				

Table 3.7. Analysis of variance for optimized response: compressive modulus.

Source	DF	Seq SS	Contribution	Adj SS	Adj MS	F-Value	P-Value
Model	2	0.5124	25.00%	0.5124	0.25621	7.00	0.002
Linear	2	0.5124	25.00%	0.5124	0.25621	7.00	0.002
HA (wt%)	1	0.3608	17.60%	0.3608	0.36085	9.86	0.003
2nd dep. angle	1	0.1516	7.39%	0.1516	0.15158	4.14	0.048
Error	42	1.5374	75.00%	1.5374	0.03660		
Lack-of-Fit	6	0.1127	5.50%	0.1127	0.01878	0.47	0.823
Pure Error	36	1.4247	69.50%	1.4247	0.03957		
Total	44	2.0498	100.00%				

Table 3.8. Analysis of variance for optimized response: Alamar Blue reduction at day 1.

Accordingly, Figure 3.5 reports the Pareto chart of the standardized effects (modulus and Alamar Blue reduction at day 1).

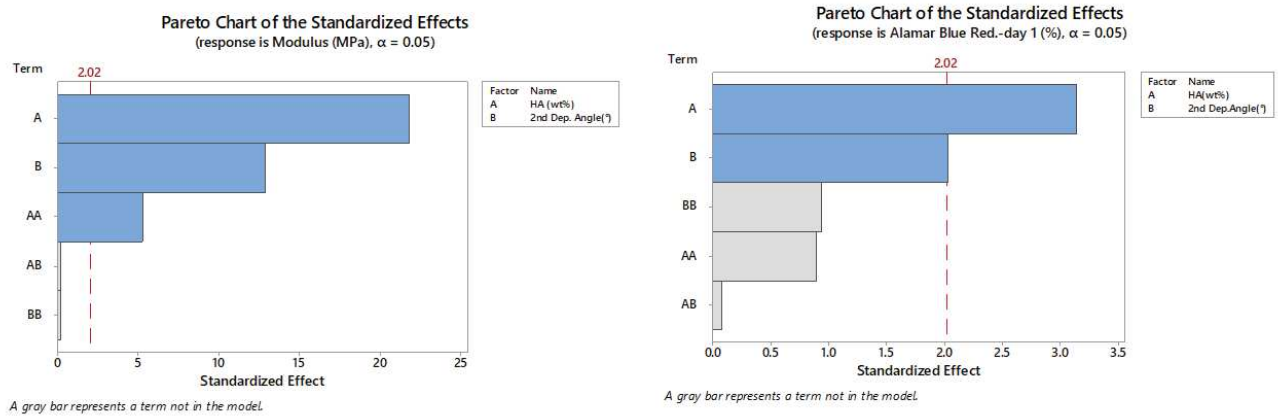

Figure 3.5. Pareto chart of the standardized effects (modulus and Alamar Blue reduction at day 1).

The three-level factorial design and the ANOVA tables led to the development of the regression models for mechanical and biological responses (Table 3.9).

RESPONSE	REGRESSION MODEL	R^2 STATISTIC
Maximum Stress (MPa)	MS = - 5.42 - 0.316C+0.2865G + 0.0454C^2- 0.001455G^2+0.00732CG	R^2= 94.6%; R^2_{adj}= 93.9%; PRESS= 42.1; R^2_{pred}= 92.8%
Modulus (MPa)	M= -2.23+0.947C+0.7342 G+0.4763C^2	R^2= 94.2%; R^2_{adj}= 93.8%; PRESS= 2546.8; R^2_{pred}= 93.0%
Alamar Blue red.-1 day (%)	ABR1 = 4.164+0.02193 C+0.00310G	R^2 =25.0%; R^2_{adj}=21.4%; PRESS= 1.8; R^2_{pred}= 14.2%;
Alamar Blue red.-3 day (%)	ABR3 = 8.903 + 0.2479 C- 0.1081G- 0.02255C^2 + 0.000981G^2+ 0.002862 CG	R^2= 96.5%; R^2_{adj}=96.0%; PRESS=3.2; R^2_{pred}=95.3%
Alamar Blue red.-7 day (%)	ABR7 = 9.167+0.3624C-0.0928G- 0.03346 C^2+0.000872G^2+0.003243CG	R^2 =96.4%; R^2_{adj}=96.0%; PRESS = 4.1; R^2_{pred}= 95.2%

Table 3.9. Regression models and R^2 statistic obtained for mechanical (compressive modulus and maximum stress) and biological responses (Alamar Blue reduction at 1, 3 and 7 days). The material composition (i.e., amount of HA) and the geometrical feature (i.e., second deposition angle) are marked as C and G, respectively.

However, the development of regression models using the ANOVA approach clearly requires a check of adequacy.

A check on the assumption related to the normal distribution for the errors was performed by considering the plots of the normal probability for the residuals from each developed model (Figures 3.6 and 3.7).

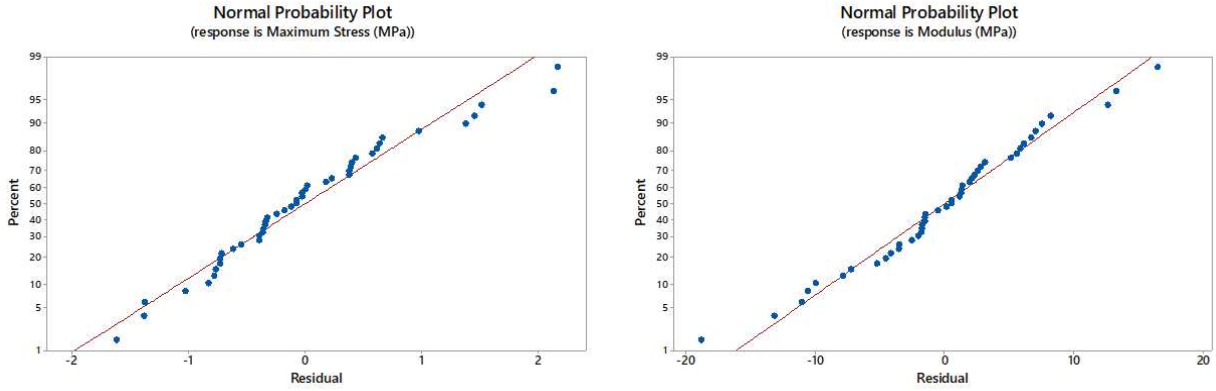

Figure 3.6. Normal probability plots of residuals for mechanical responses (maximum stress and modulus).

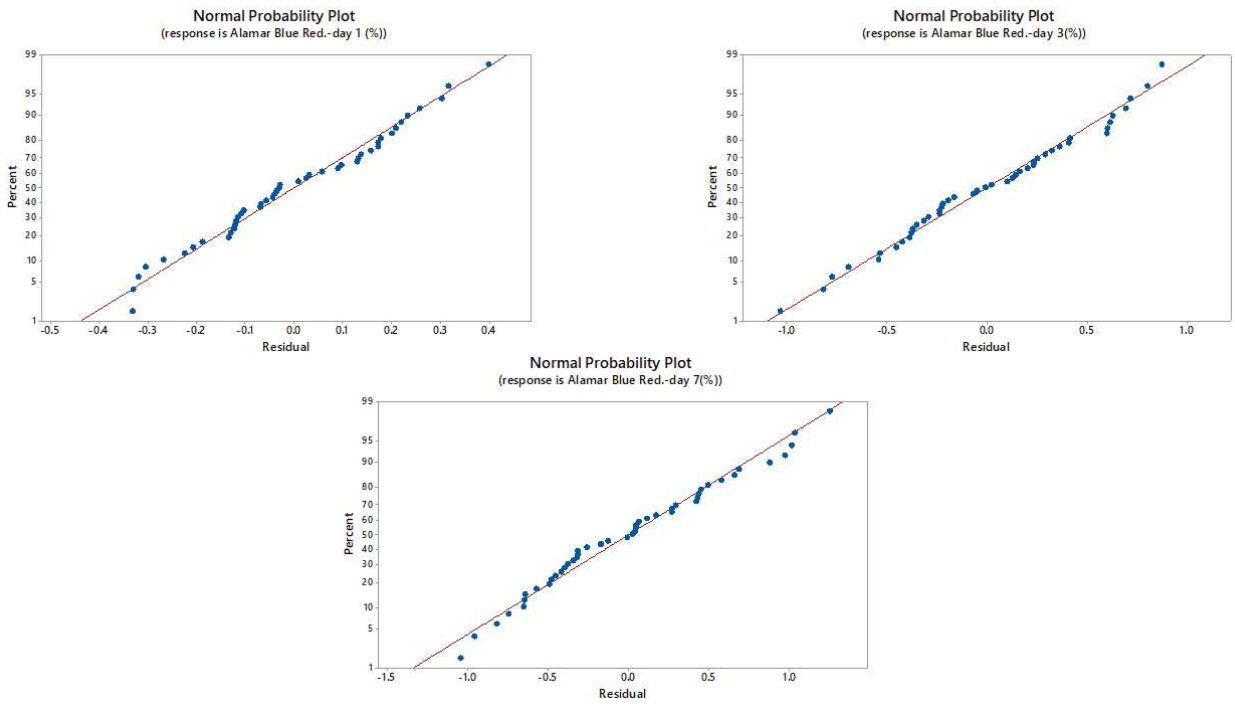

Figure 3.7. Normal probability plots of residuals for biological responses (Alamar Blue reduction at 1, 3 and 7 days).

It is worth noting how a straight line was generally followed by all residual plots, also confirming the validity of the assumption related to the normal distribution.

Concerning this method, in general a great emphasis is on the middle part of the plot rather than on the two extremes of the range, where small deviation from normality may be allowed [32,33].

The R^2 statistic generally represents a further approach to assess the applicability of the obtained models. In brief, it provides an information on the model focusing on the variation of the mean values, also indicating an overall measure of the obtained fit.

The reported values of R^2 and R^2_{adj} indicate how the obtained models fit the experimental results

Furthermore, the prediction error sum of squares (PRESS) may measure the capability of the models in predicting the mechanical and biological responses in new experimental observations and, consequently, the predicted R^2 (R^2_{pred}), which is R^2 for prediction, may be evaluated from the PRESS value for the same purpose. In Table 3.9, the values of R^2_{pred} suggest how the models can be efficiently able to predict the responses for new experiments.

Even though the normal probability plots of residuals are generally reported to analyze some features, other useful information may be obtained by further plots [33]. The plots of residuals versus fitted values (Figures 3.8 and 3.9) were considered to further check the normality assumption and/or the eventual presence of a specific pattern for the residuals with respect to a defined variable.

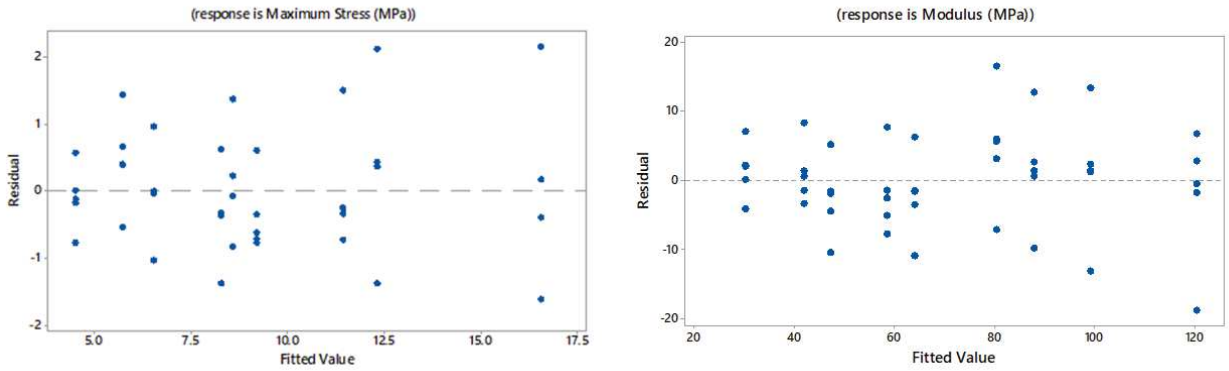

Figure 3.8. Residuals versus fitted values for mechanical responses (i.e., maximum stress and modulus).

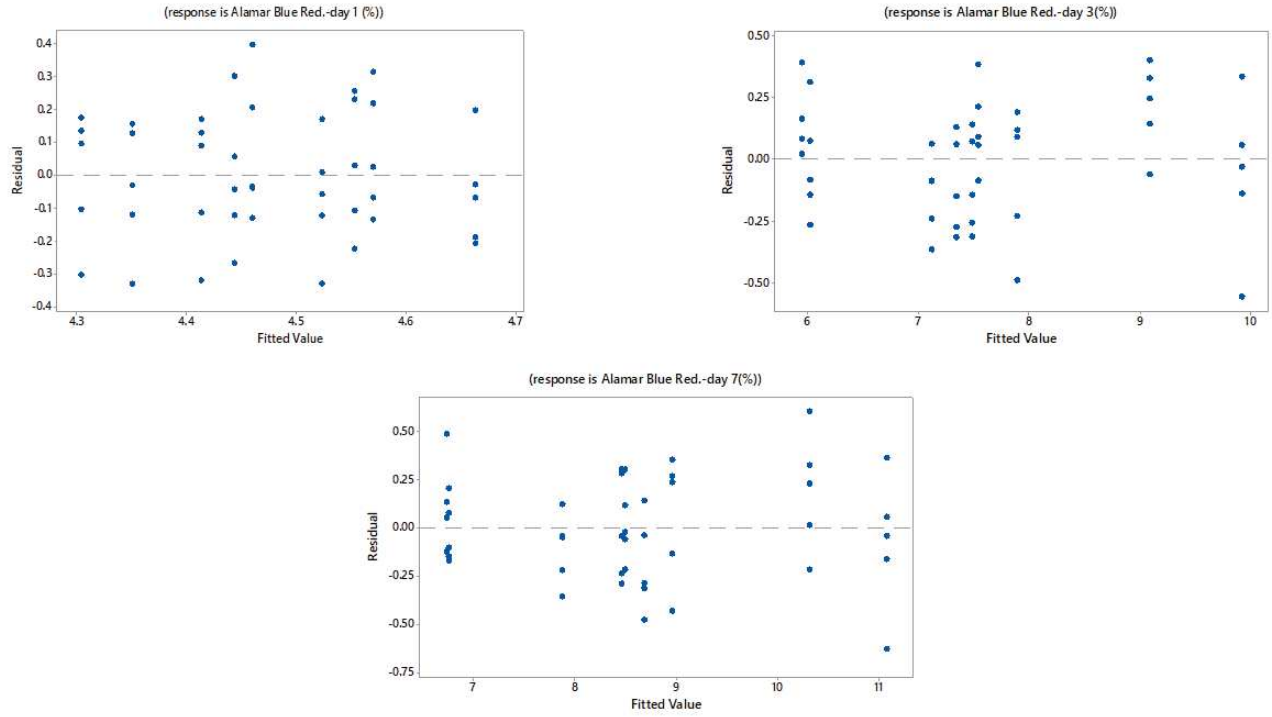

Figure 3.9. Residuals versus fitted values for biological responses (i.e., Alamar Blue reduction at 1, 3 and 7 days).

In particular, the plots of residuals versus fitted values are employed to verify the assumption related to the constant variance for the residuals.

Figures 3.8 and 3.9 reports the residuals versus fitted values for all responses. No excessively large values of the residuals were obtained for mechanical responses (i.e., maximum stress and modulus) as well as for the biological ones (i.e., Alamar Blue reduction at 1, 3 and 7 days). It seems that the obtained trends can not individuate a heteroscedastic behavior for the residuals.

In addition, with regard to mechanical and biological responses, the magnitude of the residual and the level of the variable factors (i.e., amount of HA and second deposition angle) were correlated. As for the mechanical responses (i.e. maximum stress and modulus), only a slight increase of the residuals was generally found with increasing the amount of HA and the second deposition angle (Figures 3.10). Focusing on the biological response (Figure 3.11), in the case of Alamar Blue reduction at day 1 the highest values of the residuals were obtained in the case of 5wt% of HA and second deposition angle of 60°. In general, at day 3 and day 7 a slight increase of the residuals was observed if the amount of HA and the second deposition angle were increased.

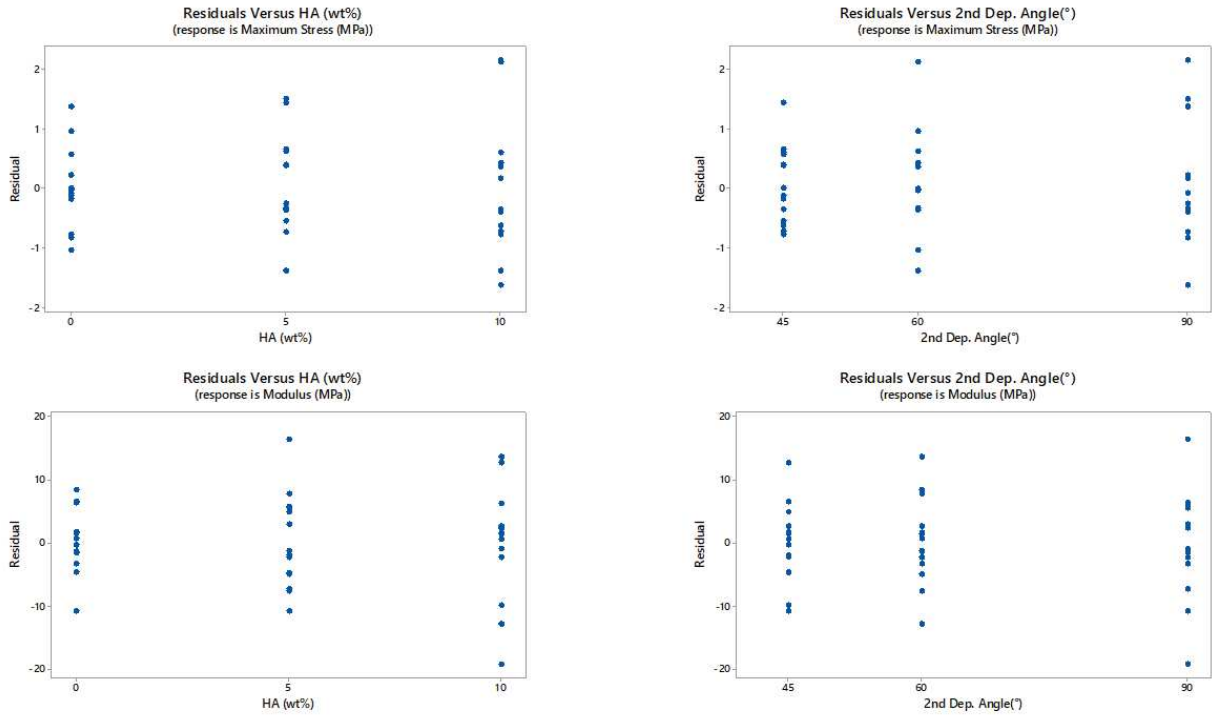

Figure 3.10. Residuals versus variable factors (i.e., amount of HA and second deposition angle) for mechanical responses (i.e., maximum stress and modulus).

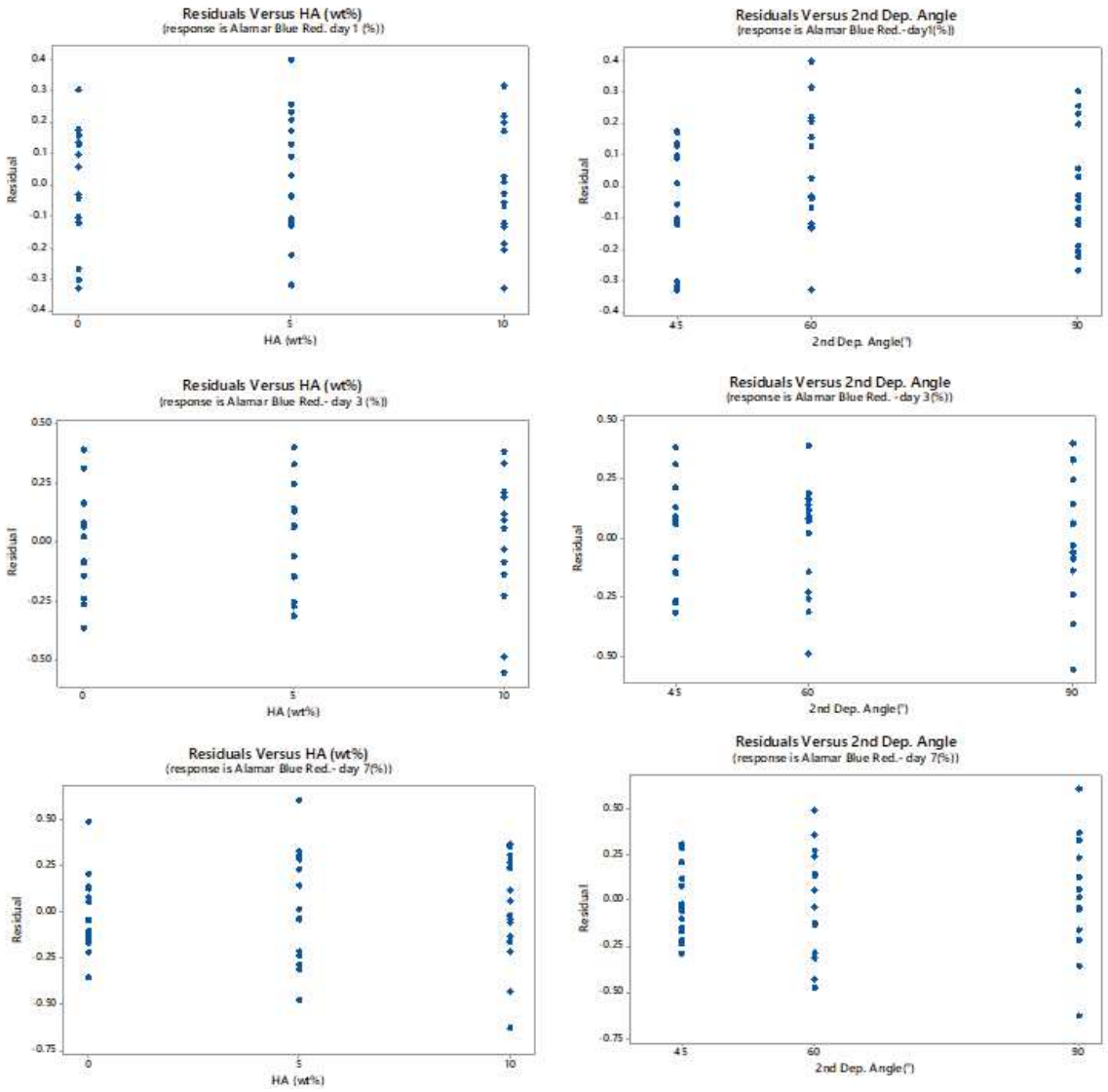

Figure 3.11. Residuals versus variable factors (i.e., amount of HA and second deposition angle) for biological responses (i.e., Alamar Blue reduction at 1, 3 and 7 days).

A graphical method was also employed to study the relationship between each mechanical (i.e., maximum stress and modulus) or biological (i.e., Alamar Blue reduction at 1, 3 and 7 days) response and the two predictor variables (i.e., amount of HA and second deposition angle) by means of a 3D surface of a predicted response. This allowed to show the regions having several properties within the analyzed level range of the variable factors (i.e., amount of HA and second deposition angle).

The response surface methodology is often employed with the aim to keep a trade-off between mechanical and functional properties as the measured responses [33]. In general, the response surface methodology may be coupled with a central composite design of experiment as an efficient design to assess the curvature of the response function [33]. This design approach may be also considered as a potential choice for the investigation of the curvature in response surfaces [33].

In the current research, a 3^2 full factorial design of two factors with three levels was considered according to the limitations on the three levels of HA and second deposition angle.

The developed models were employed to graphically report the response surfaces. The optimized solution with the desired combination of the response values was then found. Accordingly, Figures 3.11 and 3.12 report the 3D surface plots of mechanical and biological responses in terms of the variable factors as well as the 2D projections of the surfaces or the contour plots, which may be useful to define desirable response values and operating conditions.

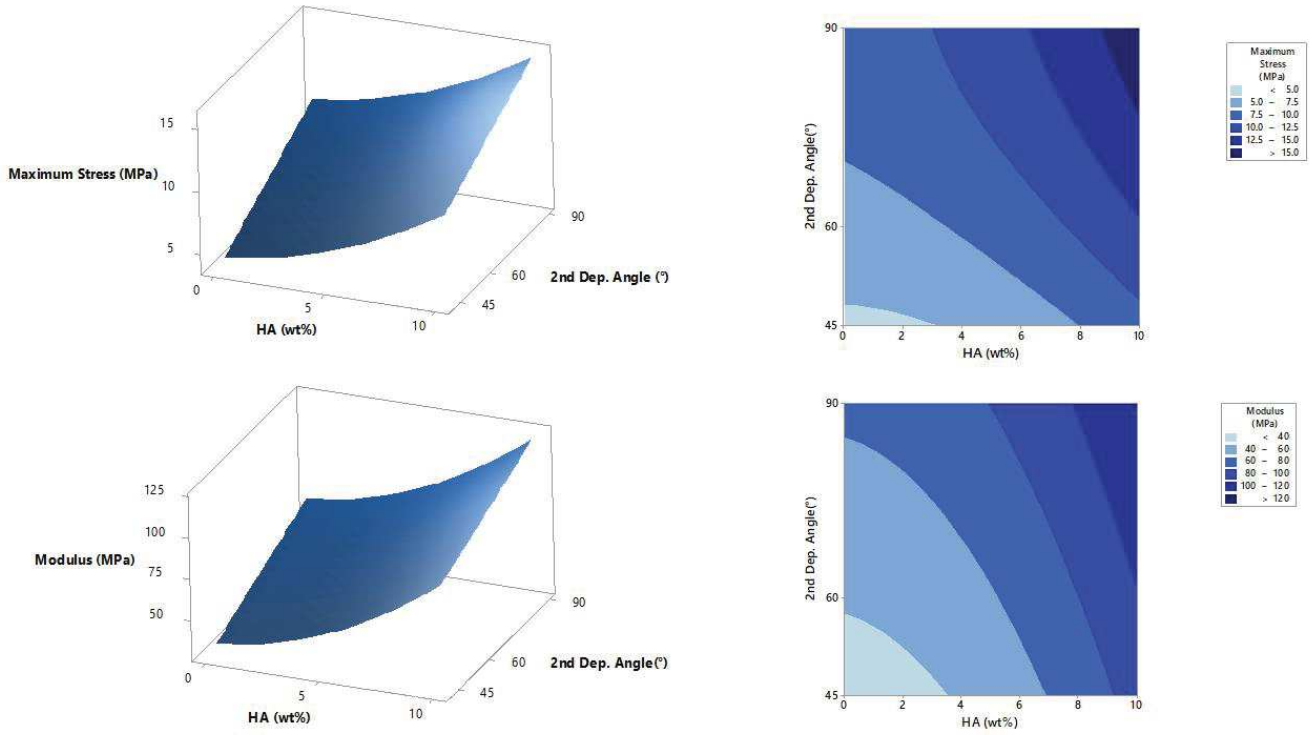

Figure 3.12. 3D surface plots and 2D contour plots of the mechanical responses (i.e., maximum stress and modulus) in the investigated domain of the variable factors.

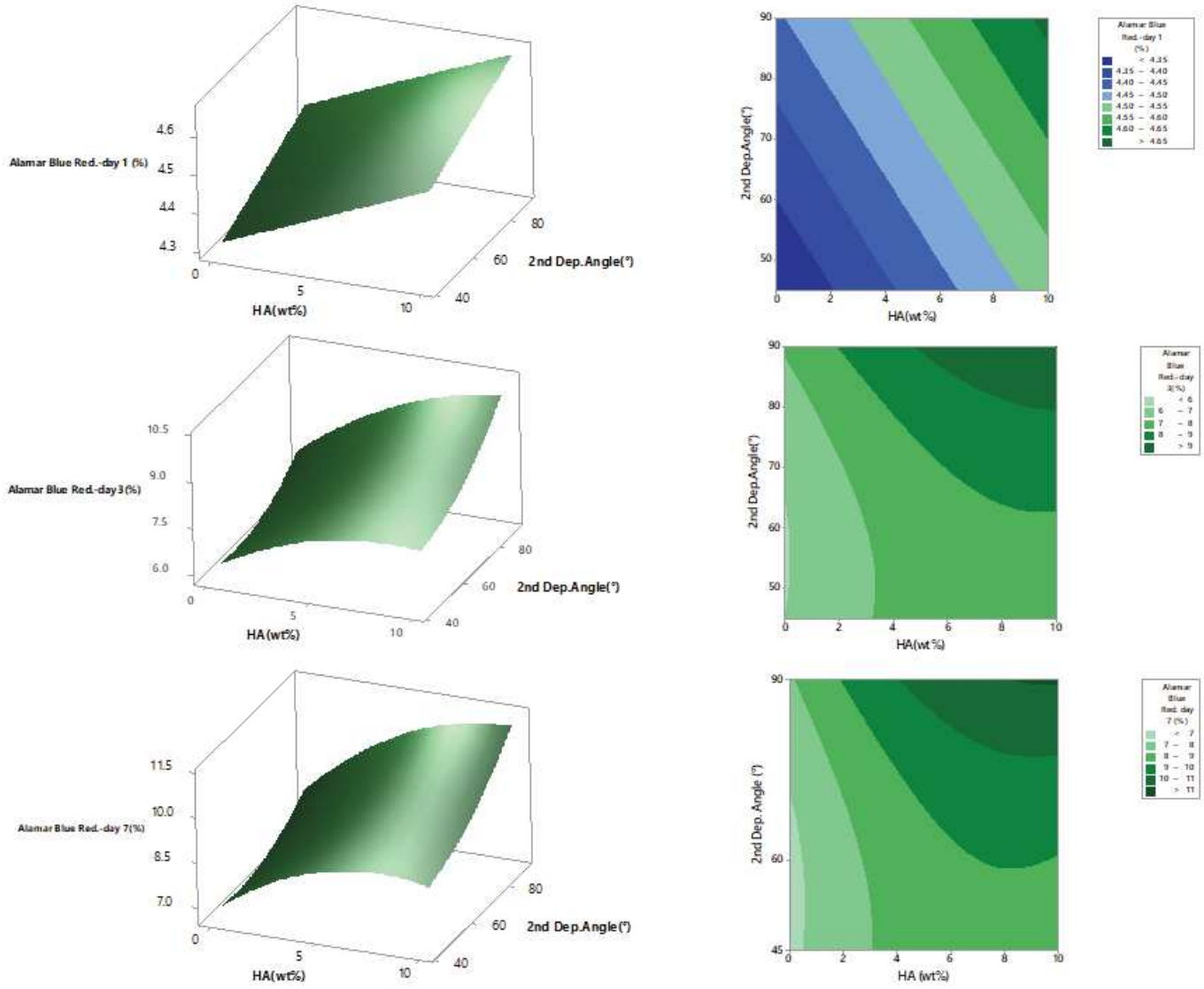

Figure 3.13. 3D surface plots and 2D contour plots of the biological responses (i.e. Alamar Blue reduction at 1, 3 and 7 days) in the investigated domain of the variable factors.

From a practical point of view, the contour plots allow to make the pattern of the responses in the investigated domain of the variable factors. It is worth noting that different patterns of responses were generated by the variable factors in the investigated region.

In general, it would be possible to find a an appropriate "formulation" of the device with desired properties benefiting from such plots. As an example, once defined the desired values for the responses, a contour plot overlay method may be adopted to find a solution with balanced properties.

However, in the current research, the composite desirability was used to assess how well the settings optimized mechanical and biological responses overall. Briefly, the composite desirability ranges from 0 to 1. A value of "0" for the desirability indicates that one or more responses are outside their acceptable limits, whereas "1" is the ideal case. Many times, in the case of multiple responses no factor setting is able to simultaneously maximize the desirability of all the responses. For this reason, the strategy involved the maximization of the composite desirability.

The composite desirability is based on the combination of the individual desirability of all the response variables into a single measure. The individual desirability for each response was calculated and weighted according to the assigned importance, which was the same for each response. The optimal solution occurred where the composite desirability achieved its maximum value.

Table 3.10 reports the predicted responses for an amount of HA ranging from 0 to 10 wt% at three values of the second deposition angle (i.e. 45°, 60° and 90°), whereas the optimal solution is summarized in Table 3.11.

Scaffold Formulation	HA (wt %)	2nd dep. angle (°)	Maximum Stress (MPa)	Modulus (MPa)	Alamar Blue red. - day 1 (%)	Alamar Blue red.– day 3 (%)	Alamar Blue red. - day 7 (%)
1	0	45	4.5	30.8	4.30	6.0	6.8
2	1	45	4.6	32.2	4.3	6.4	7.2
3	2	45	4.7	34.6	4.3	6.7	7.6
4	3	45	5.0	37.9	4.4	7.0	8.0
5	4	45	5.3	42.2	4.4	7.2	8.2
6	5	45	5.7	47.4	4.4	7.3	8.5
7	6	45	6.2	53.6	4.4	7.5	8.6
8	7	45	6.8	60.8	4.5	7.6	8.7
9	8	45	7.5	68.9	4.5	7.6	8.7
10	9	45	8.3	77.9	4.5	7.6	8.6
11	10	45	9.2	87.9	4.5	7.5	8.5
12	0	60	6.5	41.8	4.4	6.0	6.7
13	1	60	6.7	43.2	4.4	6.3	7.3
14	2	60	7.0	45.6	4.4	6.7	7.7
15	3	60	7.3	49.0	4.4	7.0	8.1
16	4	60	7.7	53.2	4.4	7.3	8.4
17	5	60	8.3	58.5	4.5	7.5	8.7
18	6	60	8.9	64.6	4.5	7.6	8.9
19	7	60	9.6	71.8	4.5	7.8	9.0
20	8	60	10.4	79.9	4.5	7.9	9.0
21	9	60	11.3	88.9	4.5	7.9	9.0
22	10	60	12.3	98.9	4.6	7.9	9.0
23	0	90	8.6	63.8	4.4	7.1	7.9
24	1	90	9.0	65.3	4.5	7.6	8.5
25	2	90	9.4	67.6	4.5	8.0	9.0
26	3	90	10.0	71.0	4.5	8.4	9.5
27	4	90	10.7	75.3	4.5	8.8	10.0
28	5	90	11.4	80.5	4.6	9.1	10.3
29	6	90	12.3	86.7	4.6	9.3	10.6
30	7	90	13.2	93.8	4.6	9.6	10.8
31	8	90	14.2	101.9	4.6	9.7	11.0
32	9	90	15.3	110.9	4.6	9.8	11.1
33	10	90	16.5	120.9	4.7	9.9	11.1

Table 3.10. Predicted mechanical and biological responses for different formulation of 3D additive manufactured PCL/HA scaffolds. The amount of HA was varied from 0 to 10 wt%

Scaffold Formulation	HA (wt %)	2nd dep. angle (°)	Maximum Stress (MPa)	Modulus (MPa)	Alamar Blue red. - day 1 (%)	Alamar Blue red.– day 3 (%)	Alamar Blue red. - day 7 (%)	Composite Desirability
33	10	90	16.5	120.9	4.7	9.9	11.1	0.9

Table 3.11. Optimal solution based on composite desirability for mechanical and biological responses.

3.4. Conclusions

An approach based on a 3^2-full factorial DOE and ANOVA was implemented with the aim to engineer the mechanical and biological properties of 3D nanocomposite PCL/HA scaffolds for hard tissue regeneration. Values of the maximum stress and modulus obtained from compression tests were the mechanical responses, whereas the Alamar Blue reduction at 1, 3 and 7 days were the biological responses. Regression models were developed for each measured response to fit the experimental data. The normality assumption of the ANOVA was validated by means of the normal probability plots of the residuals, whereas the plots of the residuals versus the fitted values or the variable factors (amount of HA, second deposition angle) provided further information.

Moreover, the R^2 statistic was reported to assess the predictability of the models. However, in the current research, the response surface methodology was not employed for effectively finding a level domain of the variable factors to achieve a scaffold formulation with balanced mechanical and biological performances. It was especially considered to visualize regions having several mechanical and biological properties in the investigated level domain of the variable factors. Accordingly, as all maximum stress, compressive modulus and Alamar Blue at different time points had to be maximized, and as in the case of multiple responses no factor setting is able to maximize the desirability of all the responses at the same time, a strategy involving the maximization of the composite desirability was adopted.

The predicted values of the mechanical and biological responses were reported for different formulations of 3D additive manufactured PCL/HA scaffolds while varying the amount of HA from 0 to 10 wt% and considering three values for the second deposition angle (i.e. 45°, 60° and 90°). Based on the composite desirability, the optimal solution (i.e. scaffold formulation N.33 - amount of HA: 10 wt%, second deposition angle: 90°), which maximized all the responses, was found starting from the predicted values.

3.5. References

[1] Langer R. and J.P. Vacanti. 1993. Tissue engineering. Science. 260(5110); 920–6.

[2] Hollister, S.J. 2005. Porous scaffold design for tissue engineering. Nat Mater. 4(7); 518-24.

[3] Thrivikraman, G., A. Athirasala, C. Twohig, S. Kumar Boda and L. E. Bertasson. 2017. Biomaterials For Craniofacial Bone Regeneration. Dent. Clin. North. Am . 61(4); 835–856.

[4] Bertassoni, L.E. and P.G. Coelho. 2015. Engineering mineralized and load bearing tissues. Springer, New York.

[5] De Santis, R., A. Gloria and L. Ambrosio. 2010. Materials and technologies for craniofacial tissue repair and regeneration. TOPICS in MEDICINE. 16 (1-4).

[6] De Santis, R., U. D'Amora, T. Russo, A. Ronca, A. Gloria and L. Ambrosio. 2015. 3D fibre deposition and stereolithography techniques for the design of multifunctional nanocomposite magnetic scaffolds. J Mater Sci Mater Med. 26(10): 250. doi: 10.1007/s10856-015-5582-4.

[7] Domingos, M., A. Gloria, J. Coelho, P. Bartolo and J. Ciurana, 2017. Three-dimensional printed bone scaffolds: The role of nano/micro-hydroxyapatite particles on the adhesion and differentiation of human mesenchymal stem cells. Proc. Inst. Mech. Eng. H. 231; 555-564.

[8] Gloria, A., R. De Santis R and L. Ambrosio. 2010. Polymer-based composite scaffolds for tissue engineering. J Appl Biomater Biomech. 8(2); 57-67.

[9] Gloria, A., T. Russo, U. D'Amora, S. Zeppetelli, T. D'Alessandro, M. Sandri, M. Banobre-Lopez, Y. Pineiro-Redondo, M. Uhlarz, A. Tampieri, A.; et al. 2013.]Magnetic poly(ε-caprolactone)/iron-

doped hydroxyapatite nanocomposite substrates for advanced bone tissue engineering. J. R. Soc. Interface. 10, 20120833.

[10] Gloria, A., Russo, T., Martorelli, M., De Santis, R. 2020. From Conventional Approaches to Sol-gel Chemistry and Strategies for the Design of 3D Additive Manufactured Scaffolds for Craniofacial Tissue Engineering. In: Current Advances in Oral and Craniofacial Tissue Engineering. CRC Press.

[11] Russo, T., A. Gloria, V. D'Antò, U. D'Amora, G. Ametrano, F. Bollino, R. De Santis, G. Ausanio, M. Catauro, S. Rengo and L. Ambrosio. 2010. Poly(ε-caprolactone) reinforced with sol-gel synthesized organic-inorganic hybrid fillers as composite substrates for tissue engineering. J. Appl. Biomater. Biomech. 8 (3); 146-152.

[12] Russo, T., et al. 2013. Systematic Analysis of Injectable Materials and 3D Rapid Prototyped Magnetic Scaffolds: From CNS Applications to Soft and Hard Tissue Repair/Regeneration. Procedia Engineering. 59; 233-239.

[13] Santis, R., A. Gloria, T. Russo, U. D'Amora, V. D'Antò, F. Bollino, M. Catauro, F. Mollica, S. Rengo and L. Ambrosio. 2013. Advanced composites for hard-tissue engineering based on PCL/organic-inorganic hybrid fillers: From the design of 2D substrates to 3D rapid prototyped scaffolds. Polym. Compos. 34; 1413–141.

[14] Sawkins, M.J., et al. 2013. Hydrogels derived from demineralized and decellularized bone extracellular matrix. Acta Biomater. 9(8);:7865–7873.

[15] Steffen, T., et al. 2001. Porous tricalcium phosphate and transforming growth factor used for anterior spine surgery. European Spine Journal. 10(2); S132–S140.

[16] Suzuki, O., et al. 1991. Bone Formation on Synthetic Precursors of Hydroxyapatite. The Tohoku Journal of Experimental Medicine. 164(1); 37–50.

[17] Tarafder, S., et al. 2013. 3D printed tricalcium phosphate scaffolds: Effect of SrO and MgO doping on in vivo osteogenesis in a rat distal femoral defect model. Biomater Sci. 1(12); 1250–1259.

[18] Tevlin, R., et al. 2014. Biomaterials for craniofacial bone Engineering. J Dent Res 93(12);1187-1195.

[19] Holt, D.J. and D.W.Grainger. 2012. Demineralized bone matrix as a vehicle for delivering endogenous and exogenous therapeutics in bone repair. Adv Drug Deliv Rev. 64(12); 1123–8.

[20] Hulbert, S.F., et al. 1970. Potential of ceramic materials as permanently implantable skeletal prostheses. Journal of Biomedical Materials Research. 4(3); 433–456.

[21] Kamakura, S., et al. 2002. Implanted octacalcium phosphate is more resorbable than beta-tricalcium phosphate and hydroxyapatite. J Biomed Mater Res. 59(1); 29–34.

[22] Kang, Y., et al. 2013. Osteogenic and angiogenic potentials of monocultured and co-cultured human-bonemarrow-derived mesenchymal stem cells and human-umbilical-vein endothelial cells on threedimensional porous beta-tricalcium phosphate scaffold. Acta Biomater. 9(1); 4906–15.

[23] Kang, Y., et al. 2015. Engineering a vascularized collagen-β-tricalcium phosphate graft using an electrochemical approach. Acta Biomaterialia. 11; 449–458.

[24] Kasten, P., et al. 2003. Comparison of human bone marrow stromal cells seeded on calcium-deficient hydroxyapatite, β-tricalcium phosphate and demineralized bone matrix. Biomaterials. 24(15); 2593–2603.

[25] Kaur, G., et al. 2014. A review of bioactive glasses: Their structure, properties, fabrication and apatite formation. J Biomed Mater Res A. 102(1); 254–74.

[26] Kinney, R.C., et al. 2010. Demineralized bone matrix for fracture healing: fact or fiction? J Orthop Trauma. 24(Suppl 1); S52–5.

[27] Klein, C.P.A.T., et al. 1985. Interaction of biodegradable β-whitlockite ceramics with bone tissue: An in vivo study. Biomaterials. 6(3); 189–192.

[28] Kolk, A., et al. 2012. Current trends and future perspectives of bone substitute materials - from space holders to innovative biomaterials. J Craniomaxillofac Surg. 40(8); 706–18.

[29] Lanzotti, A., M. Martorelli, T. Russo and A. Gloria. 2018. Design of Additively Manufactured Lattice Structures for Tissue Regeneration. Materials Science Forum. 941; 2154-2159.

[30] Russo, T., Peluso, V., Gloria, A., Oliviero, O., Rinaldi, L., Improta, G., De Santis, R., D'Antò, V. 2020. Combination Design of Time-Dependent Magnetic Field and Magnetic Nanocomposites to Guide Cell Behavior. Nanomaterials.10(3):577.

[31] Cometa, S., Bonifacio, M.A., Tranquillo, E., Gloria, A., Domingos, M., De Giglio, E. 2021. A 3D Printed Composite Scaffold Loaded with Clodronate to Regenerate Osteoporotic Bone: In Vitro Characterization. Polymers (Basel). 13(1):150.

[32] Montgomery, D. C. 2009. Design and Analysis of Experiments. Wiley, Hoboken.

[33] Zarrinbakhsh, N., Defersha, F.M., Mohanty, A.K., Misra, M. 2014. A statistical approach to engineer a biocomposite formulation from biofuel coproduct with balanced properties. J. Appl. Polym. Sci. 131, 40443.

Chapter 4

An approach toward the design of 3D customized scaffolds for large cranial defects

4.1. Introduction

Over the past years, a wide range of materials has been considered to repair cranial defects. The repair or regeneration of cranial defects involves the use of several biomaterials (i.e. polymers, composites) and strategies for the design of advanced devices [1-3]. The combination of 3D scanning, reverse engineering and additive manufacturing [4-6] represents the most recent and advanced approach for the direct fabrication of scaffolds for cranial defects. Biodegradable polymer-based scaffolds for cranial bone regeneration are generally fabricated by fused deposition modeling (FDM). A continuous thermoplastic filament (e.g. polyesters and their copolymers) may be deposited from the melt state, the scaffold porosity and pore size are determined by the geometrical and process parameters [7]. Clearly, in the prosthetic approach, which involves the use of non-degradable devices, skull growth adds a further concern. For this reason, biodegradable scaffolds for cranial bone tissue engineering are particularly important in the case of paediatric patients [2,6].

Poly(ε-caprolactone) (PCL), polylactic acid (PLA) and poly(lactic-*co*-glycolic acid) (PLGA) are the most common polyesters employed to fabricate biodegradable scaffolds for cranial bone regeneration [6-10]. PLGA scaffolds fabricated by FDM and implanted in the parietal skull defect have also shown interesting results within three weeks of *in vivo* observations in a mice model [2,11]. However, PCL is a degradable polyester which is easy to process using FDM as its melting temperature is low (60 °C) in comparison to the other polyesters. In addition, it possesses mechanical properties which are similar to those of dense spongy bone [11,12]. PCL scaffolds for cranial bone regeneration of critical-size defects were manufactured by FDM and implanted in the rabbit and human models [13,14].

However, although many progresses have been made in the development of 3D additive manufactured devices for tissue regeneration [2,7,15-21], the aim of the current study was to design 3D customized scaffolds for the regeneration of large cranial defects, combining the reverse engineering approach with additive manufacturing.

4.2. Materials and Methods

3D customized scaffolds for large cranial defects were designed. The results previously obtained from image capture and analysis techniques [1,2] were employed to create the 3D virtual model of a skull with a large cranial defect (Figure 4.1).

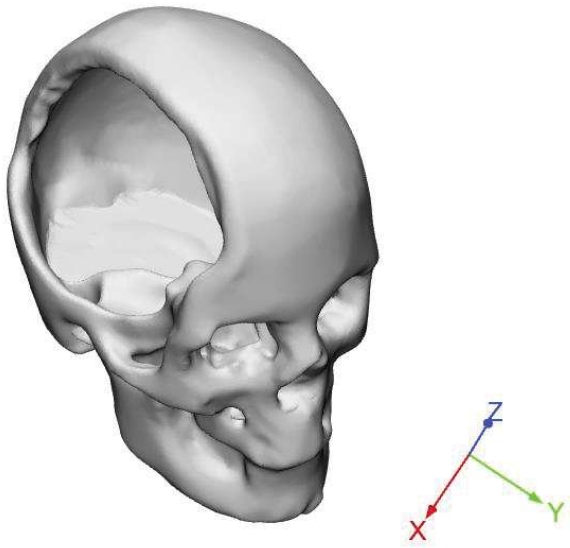

Figure 4.1. 3D reconstruction. The results obtained from a previous 3D scanning process on a skull with a large cranial defect [1] were employed, and the images were further processed.

SolidWorks®2017 (Dassault Systemes, Paris, France) computer-aided design (CAD) system was used to generate 3D customized porous scaffolds for the regeneration of large cranial defects. The starting

point was a non-porous geometrical model. A scaffold model with a porosity of about 50% was successively created (Figure 4.2).

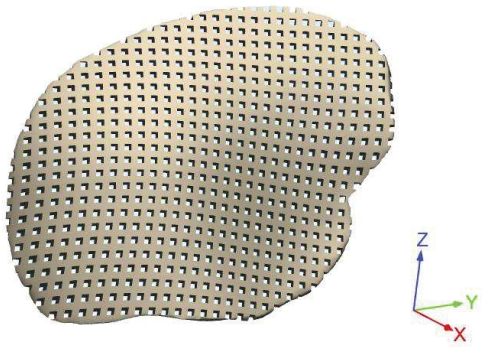

Figure 4.2. Typical geometric model of a 3D customized scaffold with interconnected pore network for large cranial defect.

The customized scaffolds consisting of PCL or PLA were also preliminarily fabricated by FDM [2]. Specifically, 3D porous scaffolds with different lay-down patterns were manufactured using a 3D printer and commercially available PCL and PLA filaments (1.75 mm in diameter). The filament was heated and the 3D customized scaffolds were built by injecting/extruding the material through a nozzle. A printing speed of about 17 mm/s was used, and the filaments were deposited according to the specific lay-down pattern. Appropriate values of the filament distance and layer thickness were selected.

4.3. Results and Discussion

Virtual models of the skull with a large defect and the 3D customized scaffolds were created. The geometry of the 3D customized scaffolds was suitably designed to be fitted in the cavity of the large defect, benefiting from the image analysis.

The feasibility of the proposed approach was preliminarily evaluated through virtual models (Figure 4.3). In brief, the potential to adapt and conform the designed scaffold to the contours of the large cranial defect was demonstrated.

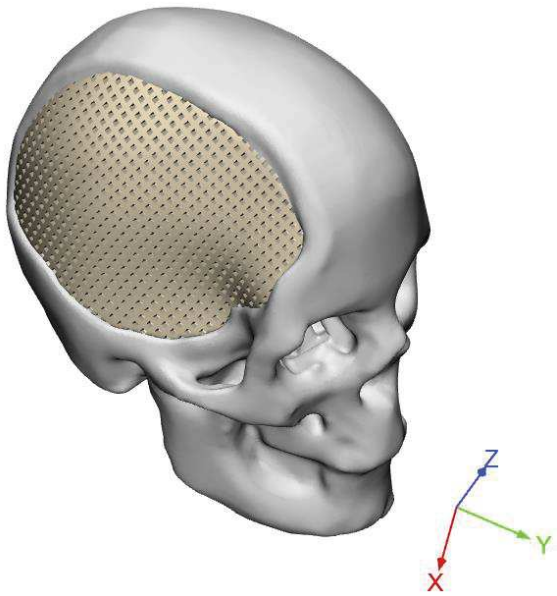

Figure 4.3. Technical feasibility of the proposed approach: an image of the virtual model of the skull with a 3D customized porous scaffold for the regeneration of large cranial defect.

4.4. Conclusions

A preliminary design of 3D customized scaffolds for large cranial defects was reported integrating the reverse engineering approach and additive manufacturing. Customized scaffolds were also additively manufactured, even if in this step the feasibility of the proposed strategy was validated through virtual models. However, the current investigation can provide a further contribution to the development of 3D customized scaffolds for large cranial defects and can be also considered as the first step of a future complex study, which will also benefit from the reported optimization strategies (Chapters 2 and 3) for the design of advanced devices.

4.5. References

[1] De Santis, R.; Gloria, A.; Ambrosio, L. Materials and technologies for craniofacial tissue repair and regeneration. Top. Med. 2010, 16, 1-6.

[2] De Santis, R.; Russo, T.; Rau, J.V.; Papallo, I.; Martorelli, M.; Gloria, A. Design of 3D Additively Manufactured Hybrid Structures for Cranioplasty. *Materials* 2021, 14, 181.

[3] Unterhofer, C.; Wipplinger, C.; Verius, M.; Recheis, W.; Thomé, C.; Ortler, M. Reconstruction of large cranial defects with poly-methyl-methacrylate (PMMA) using a rapid prototyping model and a new technique for intraoperative implant modeling. Neurol Neurochir Pol. 2017, 51(3), 214-220.

[4] Chim, H. ; Schantz, J.T. New frontiers in calvarial reconstruction: integrating computer-assisted design and tissue engineering in cranioplasty. Plast Reconstr Surg. 2005, 116(6), 1726-1741.

[5] Espalin, D.; Arcaute, K.; Rodriguez, D.; Medina, F.; Posner, M. ; Wicker, R. Fused deposition modeling of patient-specific polymethylmethacrylate implants. Rapid Prototyp J. 2010, 16(3), 164-173.

[6] Hassan, M.N.; Yassin, M.A.; Suliman, S.; Lie, S.A.; Gjengedal, H.; Mustafa, K. The Bone Regeneration Capacity of 3D-Printed Templates in Calvarial Defect Models: A Systematic Review and Meta-Analysis. Acta Biomater. 2019, 91, 1-23.

[7] Gloria, A.; De Santis, R.; Ambrosio, L. Polymer-based composite scaffolds for tissue engineering. J. Appl. Biomater. Biomec. 2010, 8(2), 57-67.

[8] Sinikovic, B.; Schumann, P.; Winkler, M.; Kuestermeyer, J.; Tavassol, F.; von See, C; et al. Calvaria bone chamber—a new model for intravital assessment of osseous angiogenesis. J. Biomed. Mater. Res. A. 2011, 99(2), 151-157.

[9] Gephart, M.G.H.; Woodard, J.I.; Arrigo, R.T.; Lorenz, H.P.; Schendel, S.A.; Edwards, M.S.B.; et al. 2013. Using bioabsorbable fixation systems in the treatment of pediatric skull deformities leads to good outcomes and low morbidity. Childs Nerv Syst 2013, 29(2), 297-301.

[10] Chao, M.T.; Jiang, S.; Smith, D.; DeCesare, G.E.; Cooper, G.M.; Pollack, I.F., et al. Demineralized bone matrix and resorbable mesh bilaminate cranioplasty: a novel method for

reconstruction of large-scale defects in the pediatric calvaria. Plast Reconstr Surg. 2019, 123(3), 976-982.

[11] De Santis, R.; Gloria, A.; Russo, T.; D'Amora, U.; Zeppetelli, S.; Tampieri, A.; et al. A route toward the development of 3D magnetic scaffolds with tailored mechanical and morphological properties for hard tissue regeneration: Preliminary study. Virtual and Physical Prototyping 2011, 6(4), 189-195.

[12] Russo, L.; Gloria, A.; Russo, T.; D'Amora, U.; Taraballi, F.; De Santis, R.; et al. Glucosamine grafting on poly (ε-caprolactone): a novel glycated polyester as a substrate for tissue engineering. RSC Adv. 2013,3(18), 6286-6289.

[13] Schantz, J.T.; Teoh, S.H.; Lim, T.C.; Endres, M.; Lam, C,X; Hutmacher, D.W. Repair of calvarial defects with customized tissue-engineered bone grafts I. Evaluation of osteogenesis in a three-dimensional culture system. Tissue eng. 2003, 9(4, Supplement 1), 113-126.

[14] Schantz, J.T.; Hutmacher, D.W.; Lam, C.X.; Brinkmann, M.; Wong, K.M.; Lim, T.C.; et al. Repair of calvarial defects with customised tissue-engineered bone grafts II. Evaluation of cellular efficiency and efficacy in vivo. Tissue eng. 2003, 9(4, Supplement 1), 127-139.

[15] De Santis R., D'Amora U., Russo T., Ronca A., Gloria A., Ambrosio L. 3D fibre deposition and stereolithography techniques for the design of multifunctional nanocomposite magnetic scaffolds. *J.* Mater. Sci. Mater. Med. 2015;26:250.

[16] Askari, M.; Naniz , M.A.; Kouhi , M.; Saberi , A.; Zolfagharian , A.; Bodaghi M. Recent progress in extrusion 3D bioprinting of hydrogel biomaterials for tissue regeneration: a comprehensive review with focus on advanced fabrication techniques. Biomater Sci 2020 Nov 13. Online ahead of print.

[17] Domingos, M.; Chiellini, F.; Gloria, A.; Ambrosio, L..; Bartolo, P.; Chiellini, E. Effect of process parameters on the morphological and mechanical properties of 3D Bioextruded poly(ε-caprolactone) scaffolds. Rapid Prototyping Journal 2012, 18, 56-67.

[18] Domingos, M.; Intranuovo, F.; Russo, T.; Santis, R.D.; Gloria, A.; Ambrosio, L.; Ciurana, J.; Bartolo, P. The first systematic analysis of 3D rapid prototyped poly(ε-caprolactone) scaffolds manufactured through BioCell printing: The effect of pore size and geometry on compressive mechanical behaviour and in vitro hMSC viability. Biofabrication 2013, 5, 045004.

[19] Gonçalves F.A.M.M.; Fonseca A.C.; Domingos M.; Gloria A.; Serra A.C.; Coelho J.F.J. The potential of unsaturated polyesters in biomedicine and tissue engineering: Synthesis, structure-properties relationships and additive manufacturing. Prog. Polym. Sci. 2017, 68, 1–34.

[20] Moxon, S.R.; Ferreira, M.J.; Santos, P.; Popa, B.; Gloria, A.; Katsarava, R.; Tugushi, D.; Serra, A.C.; Hooper, N.M.; Kimber, S.J.; Fonseca, A.C.; Domingos, M.A.N. A Preliminary Evaluation of the Pro-Chondrogenic Potential of 3D-Bioprinted Poly(ester Urea) Scaffolds. Polymers 2020, 12, 1478.

[21] Rocco, N.; Papallo, I.; Nava, M.B.; Catanuto, C.; Accurso, A.; Onofrio, I.; et al. Additive manufacturing and technical strategies for improving outcomes in breast reconstructive surgery. ACTA IMEKO 2020, 9(4), 74-79.

Dottorando	**Dr.ssa Onofrio Ilaria**
Tutor	**Prof. Vincenzo D'Antò**
Coordinatore	**Prof. Francesco Beguinot**
Corso di Dottorato	**Dottorato di Ricerca in Medicina Clinica e Sperimentale**
Ciclo	**33°**
Codice borsa	**DOT1318210 - Borsa 4**
CUP	**E62G17000000006**
Titolo Progetto	**Progettazione di scaffold 3D multifunzionali custom-made, a morfologia controllata, per la riparazione/rigenerazione dei difetti relativi a strutture cranio-facciali**

La borsa di dottorato è stata cofinanziata con risorse del
Programma Operativo Nazionale Ricerca e Innovazione 2014-2020 (CCI 2014IT16M2OP005),
Fondo Sociale Europeo, Azione I.1 "Dottorati Innovativi con caratterizzazione Industriale"